STUDIES ON THE ANODIC CHARACTERISTICS OF MANGANESE OXIDES

1980

MASAYUKI MORITA

Department of Applied Chemistry
Faculty of Engineering
Osaka University

STUDIES ON THE ANODIC CHARACTERISTICS OF MANGANESE OXIDES

1980

MASAYUKI MORITA

Department of Applied Chemistry

Faculty of Engineering

Osaka University

PREFACE

The work of this thesis was done under the guidance of Professor Dr. Hideo Tamura at Osaka University for five years since 1975.

Masayuki Morita

Suita, Osaka

January, 1980

CONTENTS

GENERAL INTRODUCTION

The functions required of electrodes are fairly easy to define. In general, the electrodes for industrial electrolysis should be: (1) a good conductor, (2) an efficient electrocatalyst for the reaction in question, (3) corrosion resistant and otherwise free from chemical attack, and (4) mechanically rigid [1]. Besides these, availability and reasonable cost are also required for the electrode materials in most cases. The substances subjecting to the anodic dissolution are particularly ruled out from possible anode materials with a few exceptions. In most cases, however, it is very difficult to ensure the sufficient chemical stability of the anodes under highly polarized conditions because of the electrochemical oxidative affinity.

An anode material satisfying most of the above requirements is the insoluble anode, so-called DSA, which has recently been introduced into the chlor-alkali industry [2]. It consists of the film of the noble metal oxides supported on the valve metal substrate such as titanium, and is excellent in the catalytic activity and in the stability for the brine electrolysis compared with the graphite anode [3]. In addition to the practical works, many fundamental ones have been performed in the chloride solutions on the electrochemical behaviours of noble metals [4,5] and their alloy [6-10] and oxides [11-22] which are main components in the DSA.

On the other hand, the development of anode materials is of special importance in water electrolysis and other electrolytic

processes, not to mention brine electrolysis, because the oxygen overvoltage is the chief cause of energy losses in such devices [23]. Thus, the DSA is expected to be applied widely to the other electrolytic fields in future, and, in fact, the oxygen evolution reaction on the DSA has been studied increasingly [24-29]. However, most of the electrocatalysts so far employed in the DSA consist of the noble metal oxides, especially ruthenium dioxide, and hence it has been desired to use the oxides of base metals from the standpoints of economy and resources.

Manganese dioxide, which is abundantly present and inexpensive, has been predominantly used in a dry cell as an active material. Therefore, its solid state properties [30] and the cathodic discharge characteristics [31] have been studied fairly in detail. However, there has been no systematic work with a view to using manganese dioxide and related oxides as anodes for electrolytic processes, in spite of the publication of the recent brief papers [32-35] and the data of activation energies for the anodic evolution of oxygen and chlorine [36].

From the above viewpoints, it was intended in this work to evaluate the use of manganese oxides as a new anode material for electrolytic processes. Thus, the manganese oxide anodes primarily containing manganese dioxide were prepared by the thermal decomposition method, and their anodic characteristics were investigated in aqueous solutions. In particular, the anodic evolution reactions of oxygen and chlorine on the manganese oxides were discussed in detail. The contents of this thesis is composed of the following four chapters.

In chapter 1, the anodic characteristics of the film-type

electrodes of manganese oxides are clarified, especially with regard to the anodic evolution of oxygen. Chapter 2 describes the study on the anodic behaviours of massive manganese oxides in order to elucidate the intrinsic properties of the manganese oxides anodes in aqueous solutions. In chapter 3, the influence of the noble metals doped in the massive manganese dioxide anode is examined on the anodic evolution of chlorine. And the electrocatalytic activities of the mixed Mn-Pd oxides for the chlorine electrode reaction are discussed in chapter 4.

Most results of the investigation presented in this thesis have already been published in the following six papers.

1. The Anodic Characteristics of Manganese Dioxide Electrodes Prepared by Thermal Decomposition of Manganese Nitrate
   M. Morita, C. Iwakura and H. Tamura,
   Electrochim. Acta, 22, 325 (1977).
2. The Anodic Characteristics of Modified Mn Oxide Electrode: Ti/RuOx/MnOx
   M. Morita, C. Iwakura and H. Tamura,
   Electrochim. Acta, 23, 331 (1978).
3. The Anodic Characteristics of Massive Manganese Oxide Electrodes
   M. Morita, C. Iwakura and H. Tamura,
   Electrochim. Acta, 24, 357 (1979).
4. The Anodic Characteristics of the Massive β-MnO_2 Doped with Noble Metals in Sodium Chloride Solution
   M. Morita, C. Iwakura and H. Tamura,
   Electrochim. Acta, 24, 639 (1979).

5. The Anodic Characteristics of Mixed Mn-Pd Oxide Electrodes

   M. Morita, C. Iwakura and H. Tamura,

   Denki Kagaku, in press.

6. The Electrocatalytic Activities of the Pd-Doped MnO_2 for the Chlorine Evolution Reaction

   M. Morita, C. Iwakura and H. Tamura,

   Electrochim. Acta, in contribution.

CHAPTER 1

THE ANODIC CHARACTERISTICS OF FILM-TYPE MANGANESE OXIDE ELECTRODES

1. INTRODUCTION

Since Konovalov et al [37] first attempted to use a manganese dioxide film as an anode for electrolytic processes, there have been some brief papers [32-35] concerning manganese dioxide film anodes supported with metal substrates such as titanium. However, no consistent information has been available for anodic characteristics of the manganese dioxide film, because its anodic properties were markedly changed by the preparative condition of the film and the substrate of the electrode.

Accordingly, in this chapter, manganese oxide (MnOx) films were prepared by thermal decomposition of manganese (II) nitrate on the metal substrates such as titanium, platinum and RuOx-coated titanium, and their anodic characteristics were investigated in aqueous solutions. Especially, the kinetics and the electrocatalytic activity for the anodic evolution of oxygen were discussed in detail.

2. EXPERIMENTAL

Film-type electrodes of manganese oxide were prepared by a thermal decomposition method [38,39]. A titanium plate (12.5 x 20 x 0.5mm) or a platinum plate (12.5 x 20 x 0.2mm) was used as a substrate. 0.1M $Mn(NO_3)_2$ in an aqueous solution was applied to one side of the substrate in several sequential coatings. After each coating, the solution was dried at a moderate temperature (below 100°C in a drying oven) and then decomposed in a furnace at 170°C for 10min. The total amount decomposed was 10^{-5}mol Mn/cm^2. The sample was cooled between each of the coatings. After the final coating, it was heated to 450°C for 1h and then cooled.

In some cases, the preliminary coatings of ruthenium oxide on a titanium substrate, or the introduction of a ruthenium oxide film as an intermediate layer into the Ti/Mn oxide interface, was accomplished by thermal decomposition of ruthenium trichloride [24]. A proper quantity of 10^{-2}M or 10^{-3}M $RuCl_3$-20% HCl aqueous solution was used for this procedure. The ruthenium oxide loadings ranged from 5×10^{-8} to 1×10^{-6}mol Ru/cm^2.

The composition of the manganese oxide was determined by X-ray diffraction method and found to be the mixture of so-called β-MnO_2 and α-Mn_2O_3. On the other hand, the principal constituent of the intermediate ruthenium oxide layer was identified as RuO_2. Hereinafter, the test electrodes will be referred to as Ti/MnOx, Pt/MnOx and Ti/RuOx/MnOx electrodes for convenience.

An all-Pyrex glass H-type cell with Teflon stoppers was

used as an electrolytic cell. The counter electrode was a platinum sheet (20 x 25mm) and the reference electrode was a hydrogen electrode (he) in the same solution, a mercurous sulfate electrode (Hg/Hg_2SO_4, 0.5M H_2SO_4), a mercuric oxide electrode (Hg/HgO, 1M KOH) or a saturated calomel electrode (sce), appropriate to the electrolytes.

Each electrolyte was prepared from special grade reagent and twice-distilled water, and was purified by electrolysis over 50h before use. All gases were purified by passing through the same train as the one described in the literature [38].

The polarization characteristics of the test electrodes were measured under the potentiostatic condition with an usual potentiostat and an electronic polyrecorder, or under the galvanostatic condition with a dc constant current power supply and a digital voltmeter. In the latter case, iR drops were corrected by using an interrupter. The current densities shown in this work will be indicated by the apparent one based on the geometric area ($1cm^2$) although the electrochemically working area of each electrode was estimated by the surface chelation method [40]. All measurements except for the experiments of the temperature dependence were carried out at 30°C.

3. RESULTS AND DISCUSSION

1. Polarization characteristics

The current-potential curves obtained potentiostatically on some Ti/MnOx electrodes in 0.5M H_2SO_4 are shown in Fig. 1.

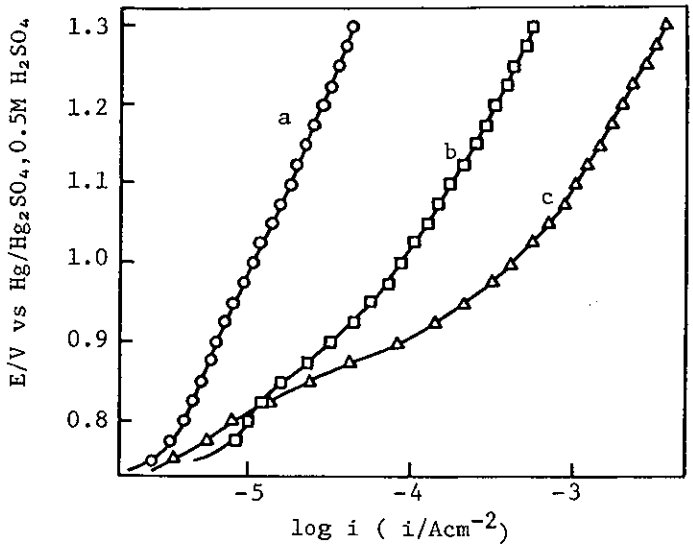

Fig. 1. Current-potential curves of Ti/MnOx in 0.5M H_2SO_4.
a: 450°C, b: 350°C, c: 250°C.

It can be seen from this figure that the anodic current decreases with increasing temperature of the final heat treatment in the electrode preparation. This temperature dependence of the current is attributable to the existence of a TiO_2 layer between the Ti substrate and the Mn oxide which is formed during the heat treatment, since it is considered that the thickness of the TiO_2 layer and then the electric resistance or the ohmic drop in the bulk of the electrode increases with increasing the temperature of the heat treatment. This interpretation was qualitatively supported by the electric resistances of these electrodes measured in mercury pool; eg Ti/MnOx (350°C): 0.62Ωcm^2, Pt/MnOx (450°C): 0.0064Ωcm^2. The existence of the TiO_2 layer, however, contributes to the adhesion of the catalytic oxide to the Ti substrate. It has been reported that β-MnO_2 which is the principal constituent of MnOx in the electrode possesses rutile structure [41] and that TiO_2 produced by thermal decomposition

has also rutile mixed with anatase [42,43]. The Ti/MnOx electrode, consequently, is superior in adhesion to Pt/MnOx, results for which are described later.

The anodic polarization characteristics of Pt/MnOx electrode are compared with that of the bright Pt electrode in Fig. 2. The Pt substrate was selected for the reason that the thick oxide film is hardly formed by the heat treatment and the electronic conductivity of the oxide is relatively high. Evidently the Pt/MnOx electrode has a considerably lower overvoltage for the oxygen evolution than the bright Pt electrode and the current at the given potential is much higher by about order two on the former than on the latter. Furthermore, anodic dissolution of the Mn oxide was not observed on a Pt/MnOx electrode. It has also become apparent that the polarization curve is scarcely affected by the change in the catalyst loading on the substrate.

Another practical approach to solve the problem of the high electric resistivity of the TiO_2 layer at the Ti/MnOx

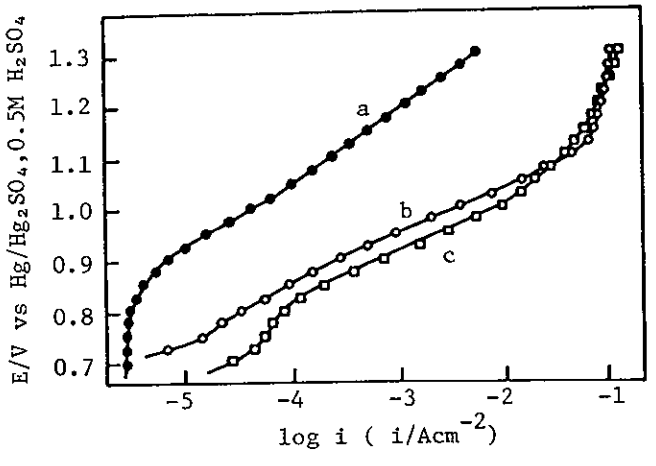

Fig. 2. Current-potential curves of Pt/MnOx in 0.5M H_2SO_4.
a: bright Pt, b: 10^{-5}mol Mn/cm², c: 10^{-4}mol Mn/cm².

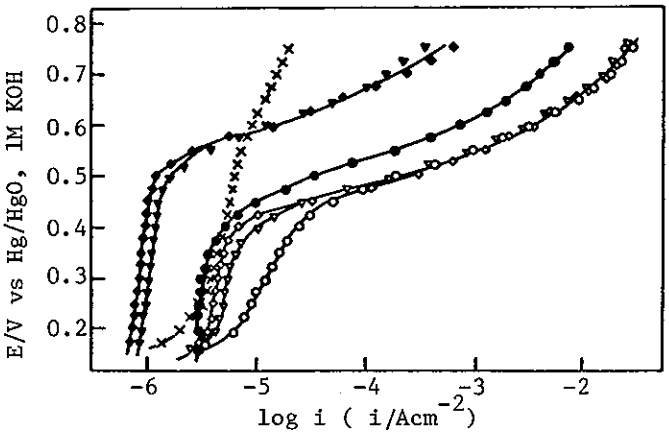

Fig. 3. Current-potential curves in 1M KOH.
○: Ti/RuOx($1x10^{-6}$)/MnOx($1x10^{-5}$),
◇: Ti/RuOx($1x10^{-7}$)/MnOx($1x10^{-5}$),
▽: Ti/RuOx($5x10^{-8}$)/MnOx($1x10^{-5}$),
●: Ti/RuOx($1x10^{-6}$), ◆: Ti/RuOx($1x10^{-7}$),
▼: Ti/RuOx($5x10^{-8}$), ×: Ti/MnOx($1x10^{-5}$).
The values in a parenthesis indicate the oxide loadings in mol/cm^2.

boundary is that the Ti substrate is covered with suitable conductive materials such as Ru oxide prior to the Mn oxide coating. Figure 3 shows the current-potential curves obtained on some Ti/RuOx/MnOx electrodes with the different amounts of Ru oxide, compared with the Ti/MnOx and Mn oxide-free Ti/RuOx electrodes. The shape of the curve and the magnitude of current density are little affected by the change in the amount of Ru oxide from 5×10^{-8} to 1×10^{-6}mol Ru/cm^2.

It is evident from this figure that the Ru oxide serves effectively as expected, since the current densities on the Ti/RuOx/MnOx electrodes are higher by a few orders of magnitude than that on the Ti/MnOx electrode. On the other hand, the current densities on the Ti/RuOx electrodes where the Ru oxide

itself acts as a catalyst for the oxygen evolution reaction are considerably lower than those on the Ti/RuOx/MnOx electrodes because of the small amounts of the RuOx catalyst. According to these results, it has become apparent that the presence of the Ru oxide decreases the electric resistivity or the potential barrier in the bulk of the electrode and that the anodic oxygen evolution occurs on the surface of the Mn oxide. In addition, it is emphasized that no anodic dissolution of the MnOx catalyst was observed in this work. For the later experiments, the amount of Ru oxide in the Ti/RuOx/MnOx electrode was kept constant at 1×10^{-7} mol Ru/cm^2.

In order to clarify how the Ru oxide contributes to the improvement of the electric characteristics in the bulk of the electrode, the in-depth analyses of the electrode constituents were carried out by means of a secondary ion mass spectrometry (SIMS). The X-ray diffraction analyses were also conducted for the oxides produced by the solid state reactions of TiO_2-MnO_2 and TiO_2-RuO_2 systems. These experimental results lead to the presumption of the composition for the metal-oxide boundary regions of Ti/MnOx and Ti/RuOx electrodes, as shown in Fig. 4. In contrast to the fact that the thermal decomposition

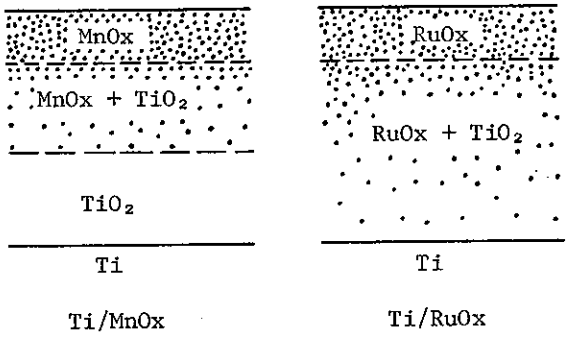

Fig. 4. Presumable models for the composition of the film-type electrodes.

of $RuCl_3$ on a titanium substrate easily leads to the formation of mixed crystals, or solid solutions, of RuOx and TiO_2 [3,16, 42,44], it seems likely that the solid solutions of MnOx and TiO_2 are difficult to be formed during the preparation of the Ti/MnOx electrode. It has been reported that β-MnO_2 is hardly soluble in TiO_2 [45].

Both RuO_2 and β-MnO_2, which are the principal constituents of Ru oxide and Mn oxide in the electrode, respectively, possess the rutile structure crystalographically. The principal constituent of the TiO_2 film formed during thermal decomposition is also rutile-type [42,43]. However, the difference in solubility for TiO_2 between β-MnO_2 and RuO_2 may related to the difference in dimension of the crystal lattice (TiO_2: a = 4.594, c = 2.958Å [46,47], β-MnO_2: a = 4.398, c = 2.867Å [47], RuO_2: a = 4.519, c = 3.116Å [46]). The volume of the unit cell of each oxide is calculated to be 62.4 for TiO_2, 55.5 for β-MnO_2 and 63.6$Å^3$ for RuO_2. Thus, the lattice dimension of TiO_2 approximately equals to that of RuO_2 but greatly differs from that of β-MnO_2. Therefore, this difficulty in the formation of solid solutions of MnOx and TiO_2 may result in the existence of a pure TiO_2 layer in the bulk of Ti/MnOx electrode, and hence the characteristics of the electrode are extremely affected by the pure TiO_2 layer which has a high resistivity and potential barrier.

Figure 5 shows the variation of potential with time during the anodic polarization at 10mA/cm^2 on a Pt/MnOx electrode in 0.5M H_2SO_4 and 1M KOH. The potential was virtually invariant, or only less than 30mV for 20h, in 1M KOH, whereas in 0.5M H_2SO_4

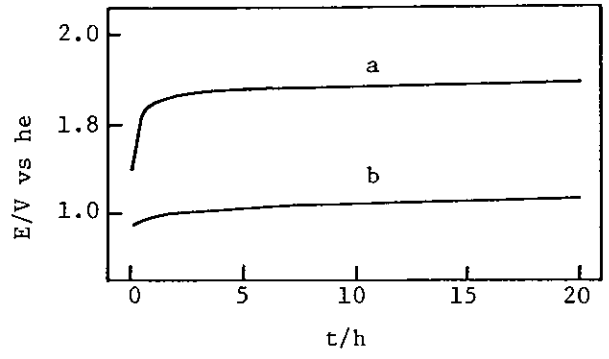

Fig. 5. Potential-time curves of Pt/MnOx under anodic polarization at 10mA/cm^2. a:in 0.5M H_2SO_4, b:in 1M KOH.

it changed to the anodic side by about 150mV during first hour after the polarization was started. Furthermore, such polarization in 0.5M H_2SO_4 resulted in weakening the mechanical bonding of the catalytic oxide, in contrast to the unchanged property in 1M KOH.

It has been suggested by Kokhanov et al [32] and Shembel' et al [33] that oxygen atoms can be incorporated into the bulk of the oxide during the anodic evolution of oxygen in acidic solutions. Then the oxygen content in the oxide of the anodized electrode was examined to clarify its connection with the variation of the electrode characteristics. In this experiment, the oxidative power, ie the content of the active oxygen, was determined [48], instead of the absolute value of the oxygen content in the oxide. The results are shown in Table 1. Evidently the oxygen content in the oxide increases by the anodic polarization in 0.5M H_2SO_4. Therefore, it seems most likely that the increase in the oxygen overpotential and the decrease in the mechanical strength with the anodic polarization,

Table 1. Active oxygen content in Pt/MnOx
(value of δ in $MnO_{1+\delta}$)

Non-anodized	Anodized for 20h	
	0.5M H_2SO_4	1M KOH
0.53	0.81 (1mA/cm^2)	0.52 (1mA/cm^2)
	0.75 (10mA/cm^2)	0.54 (10mA/cm^2)

only in acidic solutions, are associated with the increase in the oxygen content in the oxide. It has been reported that the electronic conductivity of MnO_2 increases with the increasing vacancy of oxygen [33]. Consequently, it is conceivable that the overvoltage rises with the increasing resistivity of the oxide due to an increase in the oxygen content and that the mechanical strength is reduced by the distortion of the crystal lattice due to the penetration of oxygen atoms.

The current-potential curves in the neutral solutions are shown in Figs. 6 and 7. The oxygen overvoltage in 0.5M K_2SO_4

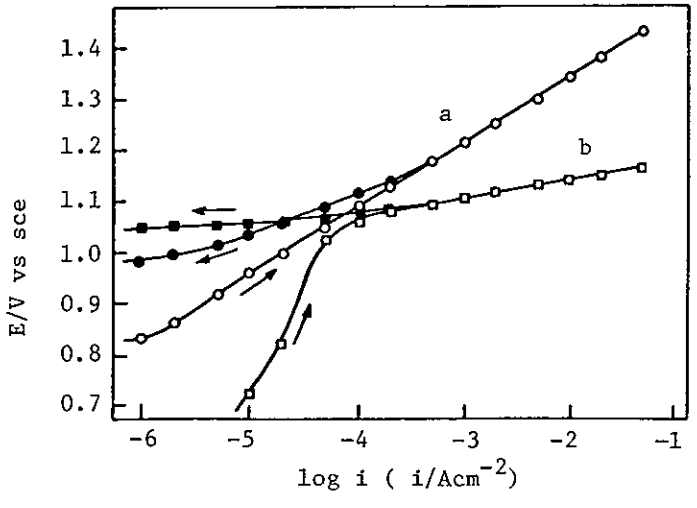

Fig. 6. Current-potential curves of Pt/MnOx in neutral solutions
a: in 0.5M K_2SO_4, b: in 1M KCl.

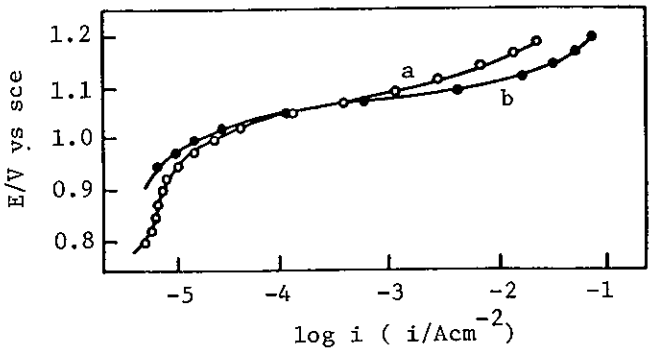

Fig. 7. Current-potential curves in 5M NaCl.
a: Ti/RuOx/MnOx, b: Pt/MnOx.

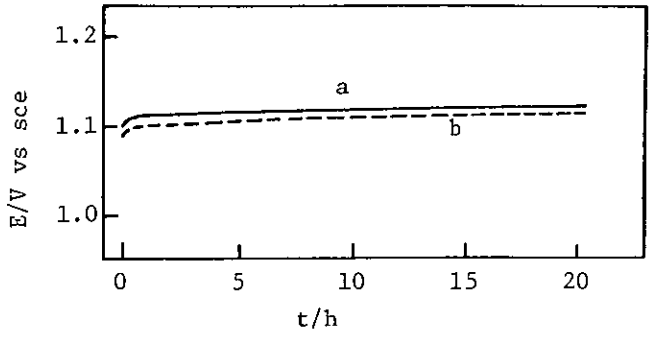

Fig. 8. Potential-time curves under anodic polarization at 10mA/cm^2 in 5M NaCl.
a: Ti/RuOx/MnOx, b: Pt/MnOx.

is rather higher than that in 0.5M H_2SO_4. Figure 8 shows the potential-time curves under anodic polarization at 10mA/cm^2. Even in solutions containing chloride ions, the electrodes remain quite stable under the anodic polarization, and chlorine evolves with low overvoltage. Hence it may be concluded that the Pt/MnOx and Ti/RuOx/MnOx are active catalysts for the chlorine evolution reaction.

2. Oxygen evolution reaction

Figures 9 and 10 show the galvanostatic polarization curves on the Pt/MnOx electrode in 0.5M H_2SO_4 and 1M KOH, respectively. From both figures, Tafel lines with the slope of 0.11V were obtained after the correction of the iR drop in the region of the high current density. The polarization curves were galvanostatically measured in the various solutions with different activities of OH^- ion prepared by diluting the original

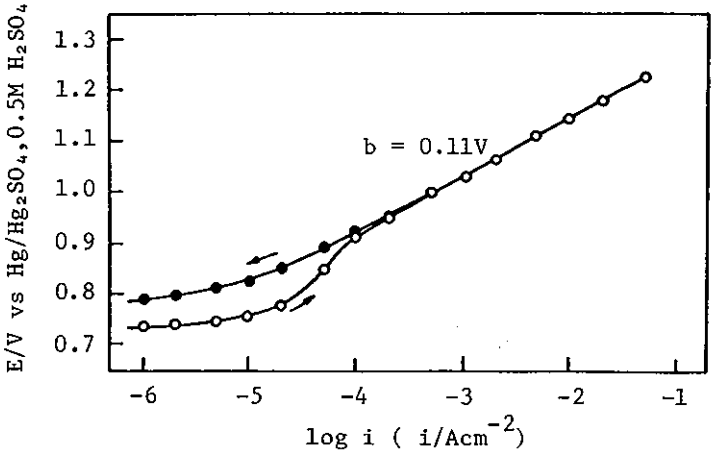

Fig. 9. Current-potential curve of Pt/MnOx in 0.5M H_2SO_4.

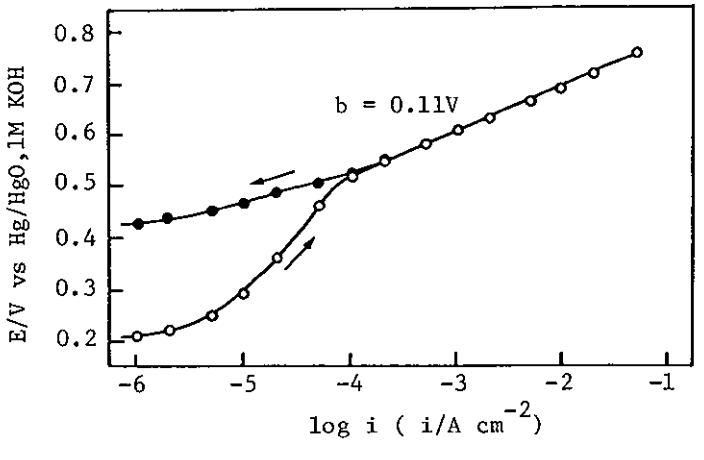

Fig. 10. Current-potential curve of Pt/MnOx in 1M KOH.

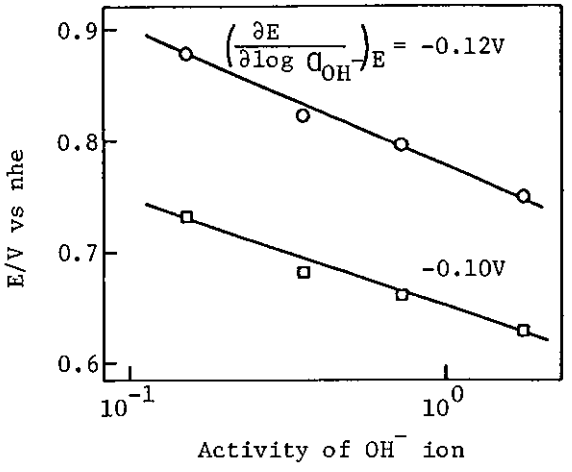

Fig. 11. Activity (a_{OH^-}) dependence of anodic potential at constant current density in KOH solutions.
o: i = 5mA/cm², □: i = 0.2mA/cm².

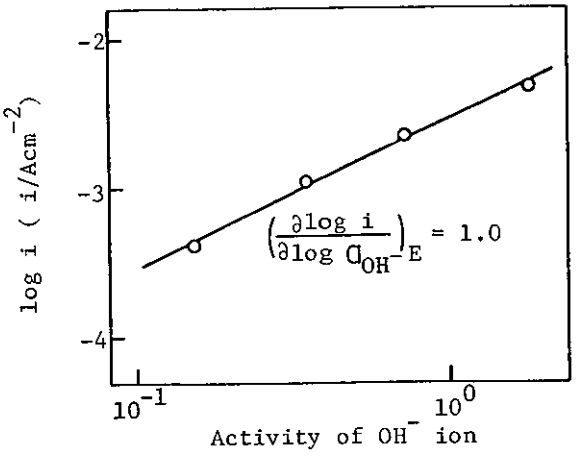

Fig. 12. Activity (a_{OH^-}) dependence of current density at constant potential (E=0.75V vs nhe).

solution of 2M KOH with twice-distilled water. From these polarization curves on the Pt/MnOx electrode, the anodic potentials at constant current density are plotted in Fig. 11 as a function of OH^- ion activity by using the activity data of KOH solution [49]. The activity dependence of current density

at the fixed potential is shown in Fig. 12. Such measurements were carried out also in the acidic solutions prepared by mixing the original solution of 0.5M H_2SO_4 and 0.5M K_2SO_4 in various ratios.

The kinetic parameters obtained from the above measurements are summarized in Table 2. Consequently, the experimental overall current density for the anodic evolution of oxygen can be formulated as

$$i = nFk\exp(FE/2RT) \qquad (1)$$

in acidic solution and

$$i = nFk'C_{OH^-}\exp(FE/2RT) \qquad (2)$$

in alkaline solution, where k and k' are the rate constants and other symbols have their usual meanings.

Any one of the oxygen reaction paths already proposed by Bockris [50] and Damjanovic et al [51] well satisfy the present data if the first step, or

Table 2. Summary of observed diagnostic criteria

	Acidic solution			
	b	$\left(\frac{\partial E}{\partial \log C_{H^+}}\right)_i$	$\left(\frac{\partial \log i}{\partial \log C_{H^+}}\right)_E$	
Experimental value	0.11V	0	0	
Idealized value	2.3 x 2RT/F	0	0	
	Alkaline solution			
	b	$\left(\frac{\partial E}{\partial \log C_{OH^-}}\right)_i$	$\left(\frac{\partial \log i}{\partial \log C_{OH^-}}\right)_E$	
Experimental value	0.11V	-0.11V	1.0	
Idealized value	2.3 x 2RT/F	-2.3 x 2RT/F	1	

$$S + H_2O \rightarrow S\text{-}OH + H^+ + e \qquad (3)$$

in acidic solution and

$$S + OH^- \rightarrow S\text{-}OH + e \qquad (4)$$

in alkaline solution are rate determining, where S stands for a site at the electrode surface. With an assumption such as these first steps being rate-controlling, the current expression in the Tafel region where the back reaction may be ignored can be written as

$$i = nFk_1 C_{H_2O} \exp(\beta FE/RT) \qquad (5)$$

in acidic solution and

$$i = nFk_1' C_{OH^-} \exp(\beta FE/RT) \qquad (6)$$

in alkaline solution, where k_1 and k_1' are the rate constants for the first steps and β is the symmetry factor. The theoretically deduced rate equations (5) and (6) are consistent with the experimentally obtained expressions (1) and (2), respectively if the usual assumption of $\beta = 1/2$ and $k_1 C_{H_2O} = k$ are made. It therefore concluded that the primary discharge step of an H_2O molecule or OH^- ion, corresponding to acidic or alkaline solution, is rate-determining in the anodic evolution of oxygen on Pt/MnOx electrode.

The galvanostatic polarization curve obtained on the Ti/RuOx/MnOx electrode in 1M KOH is shown in Fig. 13, compared with that obtained on the Pt/MnOx electrode. The anodic Tafel slope of the curve on the Ti/RuOx/MnOx electrode is b_a =

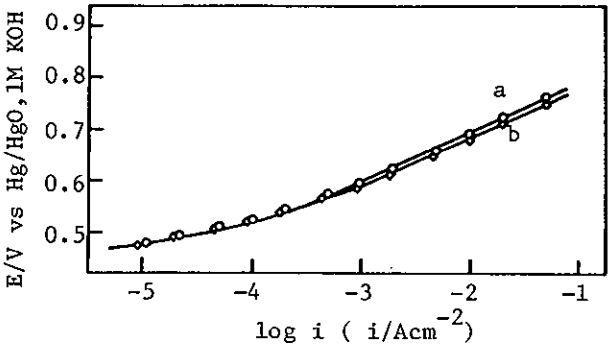

Fig. 13. Current-potential curves in 1M KOH.
a: Pt/MnOx, b: Ti/RuOx/MnOx.

0.11V the value of which is agreement with that obtained on the Pt/MnOx electrode. From the Tafel slope and other parameters for the oxygen evolution reaction, it is concluded that the oxygen evolution reaction on the Ti/RuOx/MnOx electrode in 1M KOH is also controlled by the step of the primary OH^- ion discharge, or equation (4). On the other hand, the value of b_a for the oxygen evolution reaction on the Ti/RuOx electrode in 1M KOH has been determined to be 0.04V [24]. Therefore, this difference in value of the Tafel slope supports the preceding discussion that the MnOx acts as the electrode catalyst for the anodic reaction on the Ti/RuOx/MnOx electrode. This means that the anodic evolution of oxygen takes place on the surface of the Mn oxide.

Typical Arrhenius plots at constant overvoltage for the oxygen evolution reaction on the Ti/RuOx/MnOx and Pt/MnOx electrodes in 0.5M H_2SO_4 and 1M KOH are shown in Fig. 14. An apparent activation energy can be calculated from the gradient of each straight line by using equation (7) [51,52],

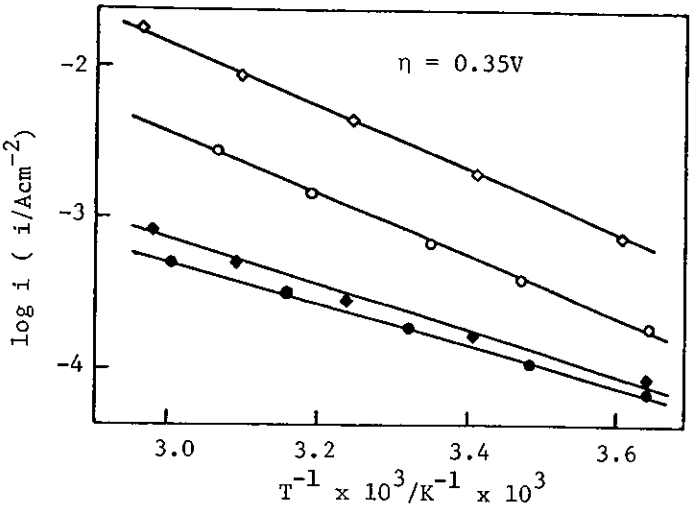

Fig. 14. Typical Arrhenius plots for O_2 evolution in 1M KOH (open symbols) and in 0.5M H_2SO_4 (closed symbols).
o,●: Pt/MnOx, ◇,◆: Ti/RuOx/MnOx.

Table 3. Apparent activation energy for the oxygen evolution reaction

	ΔH (kJ•mol^{-1})			
	Ti/RuOx/MnOx		Pt/MnOx	
overvoltage η (V)	0.5M H_2SO_4	1M KOH	0.5M H_2SO_4	1M KOH
0.25		60.2		72.7
0.35	46.0	56.8	60.6	59.4
0.45	43.9	56.4	62.3	56.9

$$\Delta H^{\ddagger}(\eta) = -2.303R(\partial \log i / \partial(1/T))_{\eta} + \alpha n F \eta \ [\text{cal/mole}] \quad (7)$$

where $\alpha n = 2.303RT/bF$, and F is a Faraday constant. Activation energies for the oxygen evolution reaction calculated from Arrhenius plots are summarized in Table 3. The substantial identity of the activation energy between on the Pt/MnOx and the Ti/RuOx/MnOx electrode is in accord with the prior results

that the mechanism of the oxygen evolution reaction on the Ti/RuOx/MnOx electrode is the same as that on the Pt/MnOx electrode. Furthermore, the values in Table 3 are also consistent with those on the bright Pt [50] and the Pt oxide [44] electrodes where the step of the primary OH^- ion discharge is rate-determining process in the oxygen evolution reaction, in agreement with the case on the Mn oxide electrodes.

The relative catalytic activity was evaluated for the oxygen evolution reaction. Roughness factors of the three kinds of electrodes under studying are summarized in Table 4. Each of roughness factor is defined as a value obtained by dividing the electrochemically working area by the apparent one. The working area can be estimated by measuring the amount of adsorption of Zn^{++} ion [40]. Considering the accuracy of the measurement of adsorption quantity, the measurement of which was carried out more than four times for each kind of electrodes, these roughness factors are regarded as the same magnitude. Furthermore, these values are comparable to that measured for DSA (Ti/RuOx) [24], and it may be, therefore, concluded that such roughness factors are one of the characteristics of the oxide electrodes prepared by the thermal decomposition in this manner. From the results in Table 4, the catalytic activity of

Table 4. Roughness factors of test electrodes

Electrode	Roughness factor
Ti/MnOx	50 - 70
Pt/MnOx	50 - 100
Ti/RuOx/MnOx	60 - 80
Ti/RuOx *	60 - 80

* Reference[24]

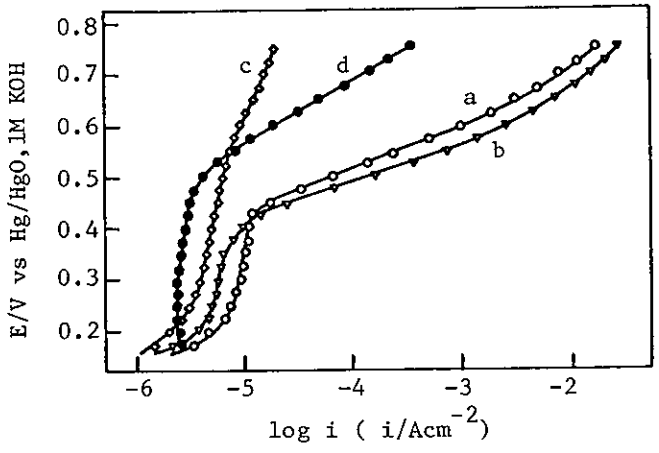

Fig. 15. Current-potential curves in 1M KOH.
a: Pt/MnOx, b: Ti/RuOx/MnOx, c: Ti/MnOx,
d: Pt.

each electrode is able to be compared by employing the apparent current density. The anodic polarization curves obtained on the Ti/MnOx, Pt/MnOx and Ti/RuOx/MnOx electrodes are shown in Fig. 15, compared with that obtained on the bright Pt electrode. Since the roughness factor of the bright Pt electrode is estimated to be more or less approximately 10, the current densities on the Pt/MnOx and Ti/RuOx/MnOx electrodes are high by 100 times or more, compared to that on the bright Pt electrode at the potential of 0.7V (vs Hg/HgO, 1M KOH). It is, therefore, apparent that the catalytic activity of the Mn oxide is much superior to that of the platinum for the anodic evolution of oxygen.

In Table 5, the oxygen overvoltage for the Ti/RuOx/MnOx electrode developed in this work is compared with those for the anode materials so far used industrially. The comparison may be made for the overvoltage at 10mA/cm^2 and 100mA/cm^2 in apparent

Table 5. Oxygen overvoltages for various anodes in 1M KOH

Anode material	Overvoltages (V) $0.01Acm^{-2}$	$0.1Acm^{-2}$
Platinum *	1.32	1.50-1.56
Platinized platinum *	0.66	0.89-0.90
Graphite *	0.96-0.98	1.12-1.17
Nickel *	0.75-0.76	0.91-0.93
Lead *	0.97	1.02-1.04
DSA (RuOx) **	0.22	0.27
DSA (IrOx) ***	0.28	0.32
Ti/RuOx/MnOx	0.40	0.51

* Reference[53]
** Reference[24]
*** Reference[26]

current density. The overvoltage for the Ti/RuOx/MnOx electrode is higher by 100 - 200mV than that for DSA being developed recently, but much lower than those for the other conventional anode materials such as graphite and nickel.

Though Mn oxide is somewhat inferior to Ru oxide and Ir oxide in the catalytic activity, the material of the Mn oxide electrode is abundantly present and inexpensive. Therefore, it may be expected that Mn oxide can practically be used as an anode in some electrolysis industries.

4. SUMMARY

The anodic characteristics of the film-type manganese oxide (MnOx) electrodes, prepared by thermal decomposition of manganese

nitrate solution, were studied in aqueous solutions. The results obtained in this chapter are summarized as follows.

1. The Ti/MnOx electrode had a high resistivity due to a thick TiO_2 film, despite strong adhesion between the oxide film and the Ti substrate.

2. The anodic characteristics were improved by replacing Ti with Pt or RuOx-coated Ti as a substrate. That is, the Pt/MnOx and Ti/RuOx/MnOx electrodes showed good anodic characteristics with a relatively low overvoltage for oxygen evolution.

3. On the MnOx film electrodes, the primary water or hydroxide ion discharge step is rate-determining in the anodic evolution of oxygen.

4. Evaluation of the catalytic activity showed that the MnOx is among the most active materials for anodic evolution of oxygen, except for some noble metal oxides, and that the Ti/RuOx/MnOx electrode would be useful for water electrolysis.

CHAPTER 2

THE ANODIC CHARACTERISTICS OF MASSIVE MANGANESE OXIDE ELECTRODES

1. INTRODUCTION

In chapter 1, it was suggested that the manganese oxide film electrodes prepared by the thermal decomposition method act as an effective catalyst for the anodic evolution of oxygen and chlorine. However, this type of electrode revealed the different characteristics depending on the kind of substrate materials. Therefore, in this chapter, the massive manganese oxide was synthesized and its anodic polarization characteristics were investigated for the purpose of eliminating the various factors influenced by substrates.

No electrochemical study of massive manganese oxides has been carried out except for the recent work by Naumann et al [54], in which the β-MnO_2 was regarded as a degenerated n-type semiconductor in the aqueous solution systems despite of the electrode reaction of the oxide itself. In the present work, the anodic polarization behaviours of the β-MnO_2 and the relating manganese oxide were investigated over the wide potential region. And then, the relationship between the electrochemical properties and the oxide compositions of the manganese oxide anodes were clarified.

2. EXPERIMENTAL

1. Preparation of test electrodes

The preparative procedure of the massive manganese dioxide was almost the same as that reported by Wiley and Knight [55]. A portion of 1.0ml $Mn(NO_3)_2$ aqueous solution (50vol.%) was introduced in the test tube of 10mm diameter, and thermally decomposed at 170 ± 10°C in air. After cooling, the additional 1.0ml $Mn(NO_3)_2$ solution was applied to the decomposed product in the bottom of test tube and then decomposed in the same condition. By repeating these procedures 5 times, about 5g of the massive product was obtained. The sample was taken out from the test tube and held in the electric furnace at 170 ± 2°C for about 20h, in order to completion of the thermal decomposition. By polishing with emery papers, the tablet-shape oxide of 9mm diameter and about 2mm thickness was prepared.

The tablets were then thermally treated at various temperatures for 6 - 20h. The resulting samples were appreciably porous so that the waterproof treatment was performed for the tablets by impregnating with polystyrene resin dissolved in benzene solvent. Both planes of tablet were polished again, and a Pt wire lead was then connected to the one side of tablet with silver paste. The other side was exposed to solution as the test plane, the remainder masked off by an insulating resin.

2. X-ray and chemical analyses

The oxide composition of the thermally treated tablets were determined by the X-ray diffraction method. The

Table 6. Test electrodes

	Heat treatment		X-ray analysis	Chemical analysis (O/Mn)	Specific resistance (Ωcm)	Classification
	Temp.(°C)	Time(h)				
1	Non-treated		β-MnO_2	2.00	0.12	A
2	460	20	β-MnO_2	2.00	—	A
3	470	20	β-MnO_2	—	—	A
4	480	6	β-MnO_2	—	—	A
5	480	20	β-MnO_2 + α-Mn_2O_3	1.97	1.1	B
6	490	20	β-MnO_2 + α-Mn_2O_3	1.62	1.7-3.0	B'
7	500	20	α-Mn_2O_3	1.61	5.3-8.0	C

diffraction pattern of the oxide without the heat treatment showed that of the β-MnO_2. In addition, the chemical analysis was carried out by the iodide method reported by Kang et al [48].

The results of these analyses were shown in Table 6, together with the sepecific resistances measured by the four-probe method. The temperatures were controlled within an error of ±2°C. The chemical compositions of the test electrodes heated below 470°C are the same as that of non-treated one, and those oxides are composed of polycrystal β-MnO_2. The values of the specific resistance are in reasonable agreement with that reported previously [55,56]. By the heat treatment above 480°C, a part of β-MnO_2 is decomposed to form the mixed oxide with α-Mn_2O_3. However, the heat treatment to more extent is necessary for the complete change in composition because of the voluminousness of the sample. The most of β-MnO_2 changes to α-Mn_2O_3 by heat-treating at 500°C for 20h. Based on the oxide composition, hereinafter, these electrodes are conveniently divided into four groups; A, B, B' and C as shown in the table.

3. Electrochemical measurements

The polarization characteristics of the test electrodes were measured in aqueous solution of 0.5M H_2SO_4, 0.5M K_2SO_4, 1M HCl, 1M KOH, 3M NaCl and 2M KBr at 30°C, and the mixed solutions of two kinds of electrolyte were used for the determination of the reaction order. The reference electrode was a hydrogen electrode (he) in the same solution or a saturated calomel electrode (sce). The other experimental procedures were same as those described in the previous chapter.

3. RESULTS AND DISCUSSION

1. Diffusion process of proton in the massive Mn oxides

The typical cyclic voltammograms in 0.5M H_2SO_4 are shown in Fig. 16, where (A) and (B) indicate the electrodes without the heat treatment and with the treatment at 480°C for 20h, respectively. The large capacitance-like currents appeared over the whole potential region in Fig. 16 is the characteristic behaviour for the manganese dioxide electrode. Such voltammograms were also observed for the RuO_2 and IrO_2 electrodes prepared by the thermal decomposition method [26, 57].

The current densities of the anodic peaks at approximately 1.5V vs he in the electrode A and B were dependent on the rate of the potential sweep and independent on the stirring of the electrolytes. The plots of the peak current densities, i_p, against the square root of the sweep rate, $v^{1/2}$, are straight line, as shown in Fig. 17. These linear relations follow the

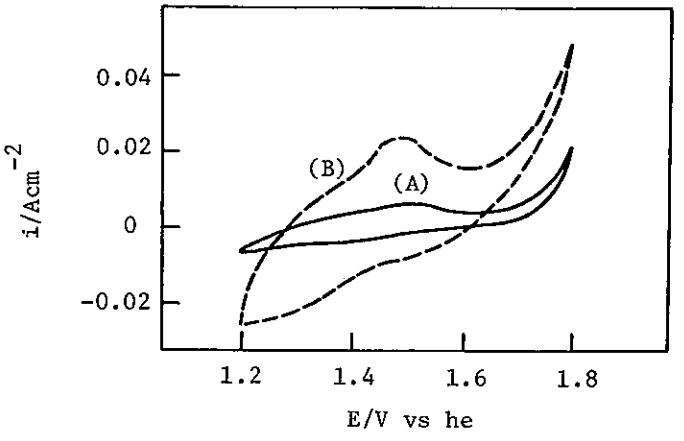

Fig. 16. Cyclic voltammograms of massive Mn oxides in 0.5M H_2SO_4.
(A): non treated, (B): heat treated at 480°C for 20h. Sweep rate: $0.1Vs^{-1}$.

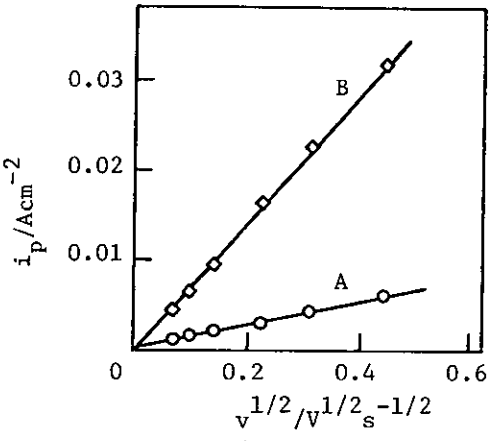

Fig. 17. i_p *vs* $v^{1/2}$ plots obtained from cyclic voltammograms.
A: electrode A, B: electrode B

theoretical equation derived from the assumption of the linear diffusion for reactant in the solution [58],

$$i_p = k_1 C° D^{1/2} v^{1/2} \quad , \tag{8}$$

where C° and D are the bulk concentration and the diffusion

coefficient of the reactant, respectively, and k_1 is the proportionality constant.

On the other hand, when the constant anodic current was applied to these electrodes, the potentials were changed in such a manner as

$$E = E_r + k_2 t^{1/2} \quad , \tag{9}$$

where E_r and k_2 are the rest potential of the electrode and the proportionality constant, respectively. The $E\text{-}t^{1/2}$ plots at the various anodic currents are shown in Fig. 18 for electrode B. Such changes in potentials are explained by the theoretical equation (10) [59],

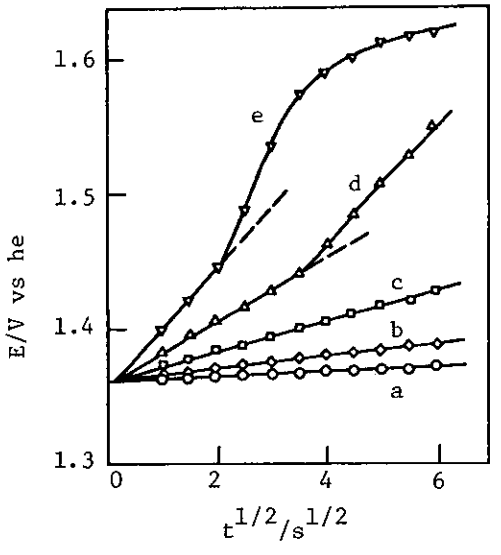

Fig. 18. Potential-time curves at constant currents in 0.5M H_2SO_4 for electrode B ($S = 0.64cm^2$).
a: at 0.05mA, b: 0.1, c: 0.2,
d: 0.5, e: 1.0.

$$\eta = E - E_o = \frac{RT\ i}{nF\ A}\left[\frac{2t^{1/2}}{nF\pi^{1/2}}\left(\frac{1}{C_x^o D_x^{1/2}} + \frac{1}{C_y^o D_y^{1/2}}\right) + \frac{1}{i_o}\right] , \qquad (10)$$

where the subscripts x and y indicate the oxidized and reduced species, respectively, and other symbols have their usual meanings.

Strictly speaking, the equations (8) and (10) are valid for reaction in the solution, but the results shown in Figs. 17 and 18 suggest that the reaction involving the diffusion process in the solid seems to follow those equations because the oxidation of Mn oxides proceeds in homogeneous solid phase [31]. It is also suggested that the anodic currents under the relatively low polarization of Mn oxide electrodes are attributed to the diffusion process of H^+ ions in the oxides. The H^+ ions in the Mn oxides, produced by the attachment of the combined water to the manganese (III) oxides, is considered to participate in the following reaction

$$MnOOH \rightarrow MnO_2 + H^+ + e \ . \qquad (11)$$

This is the reverse reaction of the first step in the cathodic discharge processes in the general form [31].

From equation (10), one obtains

$$d\eta/dt^{1/2} = \frac{2RTi}{(nF)^2\pi^{1/2}A}\left(\frac{1}{C_x^o D_x^{1/2}} + \frac{1}{C_y^o D_y^{1/2}}\right) \ . \qquad (12)$$

Hence, the value of $(1/C^\circ_x D_x^{1/2} + 1/C^\circ_y D_y^{1/2})$ can be estimated from the slopes of the straight lines shown in Fig. 18. Figure 19 shows the $d\eta/dt^{1/2}$ - i relation for the electrode A and B. From their slopes and the relation,

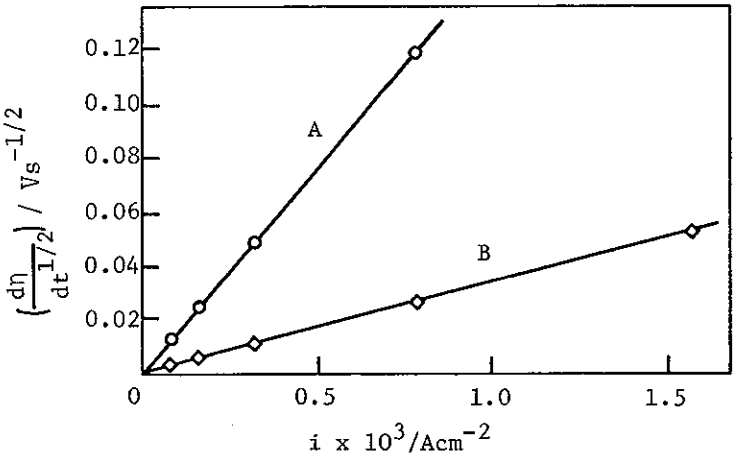

Fig. 19. $d\eta/dt^{1/2}$ *vs* i plots obtained from potential-time curves.
A: electrode A, B: electrode B.

$$1/C_x^\circ D_x^{1/2} \ll 1/C_y^\circ D_y^{1/2} \qquad (13)$$

x: H^+ in electrolyte

y: H^+ in electrode (MnOOH),

the value of $C_H^\circ + D_H^{1/2}$ in the oxide are calculated to be 5.05 x 10^{-8} for electrode A and 1.11 x 10^{-8} mole $cm^{-2}s^{-1/2}$ for electrode B. As the concentration of MnOOH in the bulk of the manganese dioxide is regarded as 10^{-3} - 10^{-4} mole cm^{-3} [39,60], the diffusion coefficient of H^+ ion, D_{H^+}, in the manganese dioxide is estimated to be 10^{-8} - 10^{-10} cm^2 s^{-1}. This value of D_{H^+} is in substantial agreement with that reported by Larange and Brenet for the polycrystalline γ-MnO_2 (8 x 10^{-8} cm^2 s^{-1}) [61], whereas it is considerably higher than that obtained by Scott for the powdered γ-MnO_2 (1.2 x 10^{-18} cm^2 s^{-1}) [62]. Furthermore, the quantity of electricity consumed during the anodic charging is calculated to be about 10mC cm^{-2}, which

corresponds to the charging in the several ten layers of the oxide electrode. These experimental results consequently suggest that these Mn oxides are easily oxidized and reduced, accompanied by the transfer of the H^+ ion in the layers near the surface.

2. Anodic evolutions of oxygen and chlorine on massive Mn oxide

The potentiostatic polarization curves in 0.5M H_2SO_4 are shown in Fig. 20. The measurements were carried out with the direction from more anodic potential to lower one, and the majority of the observed currents were assigned to the anodic evolution of oxygen. It is evident that α-Mn_2O_3 contributes to the activity for the oxygen evolution reaction, since the current density on electrode B is higher by one order of magnitude or more than that on electrode A at the same potential.

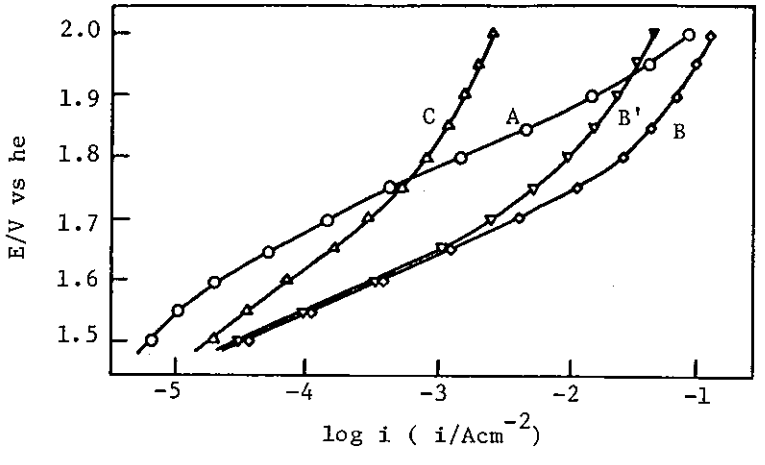

Fig. 20. Potentiostatic current-potential curves in 0.5M H_2SO_4.
A: non-treated, B: heat treated at 480°C for 20h,
B': at 490°C for 20h, C: at 500°C for 20h.

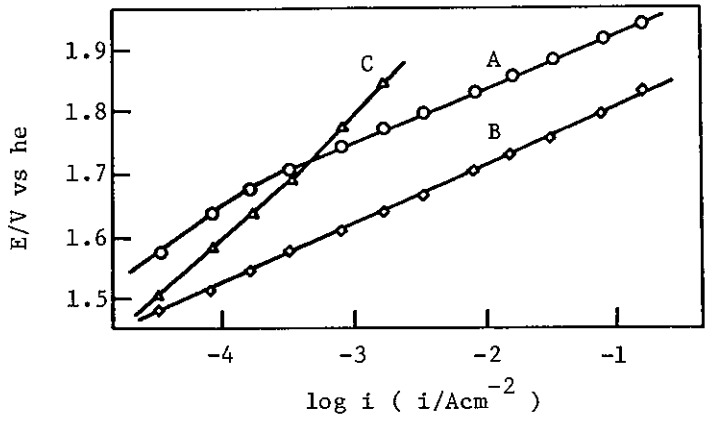

Fig. 21. Galvanostatic current-potential curves in 0.5M H_2SO_4.
A: electrode A, B: electrode B, C: electrode C.

Comparing the polarization curve of the electrode B with those of electrode B' (heat-treated at 490°C) and electrode C (heat-treated at 500°C), it is apparent that the thermal treatment at higher temperature causes the decrease of the current density. This phenomenon is due to the ohmic loss in the oxides, since the contents of α-Mn_2O_3, and then the electric resistivities, increase with the elevation of temperature in thermal treatment. Figure 21 shows the galvanostatic polarization curves in which iR correction were made for electrodes A, B and C in 0.5M H_2SO_4. The same value, 0.11V, of the Tafel slopes are obtained for both electrodes A and B, which coincides with the value for the film-type electrodes, Pt/MnOx and Ti/RuOx/MnOx, in chapter 1.

The degree of the anodic dissolution of the test electrodes were extremely small as a whole, but a clear difference was detected between the rates of the dissolution reactions for electrodes A and B. The current efficiencies of the anodic dissolutions for the three kinds of electrodes were measured at

Table 7. Current efficiency for anodic dissolution of the massive electrodes in 0.5M H_2SO_4.

Current	Current efficiency* (%)		
(mA/0.64cm^2)	A	B	C
10	$<10^{-4}$	0.090	——
20	$<10^{-4}$	0.120	——
50	$<10^{-4}$	0.265	——
100	0.002	0.151	0.083

* For the reaction, Mn(III) → Mn(VII) + 4e.

different current densities and are summarized in Table 7. In this case, the values were calculated from the dissolved quantity determined, with the assumption of four-electron oxidation. From the fact that the rate of dissolution of electrode A is much smaller than that of electrode B, it is strongly suggested that the anodic dissolution reaction proceeds at the Mn(III) site of the electrode surface. Furthermore, if the dissolution takes place through the same intermediate as the oxygen evolution on these Mn oxides, it may be considered that the Mn(III) site is rather active more than the Mn(IV) site for the anodic evolution of oxygen.

The iR-corrected polarization curves in 1M KOH and 3M NaCl solutions are shown in Figs. 22 and 23, respectively. The shape of the curves in Fig. 22 is similar to that obtained on the film-type electrodes such as Pt/MnOx and Ti/RuOx/MnOx electrodes. For the reaction of chlorine evolution, however, the massive Mn oxide electrodes revealed the behaviour different from the film-type electrodes (see Pt/MnOx in Fig. 23).

The chlorine evolution reaction in the acidic solution

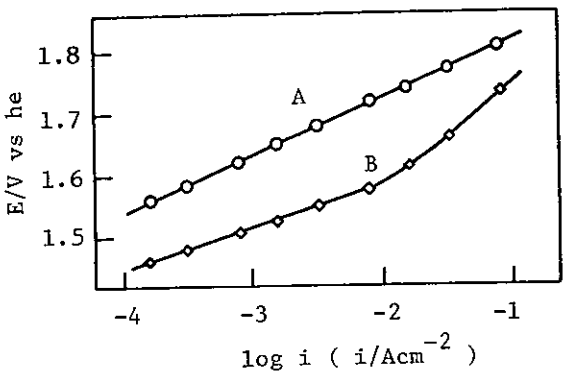

Fig. 22. Current-potential curves in 1M KOH.
A: electrode A, B: electrode B.

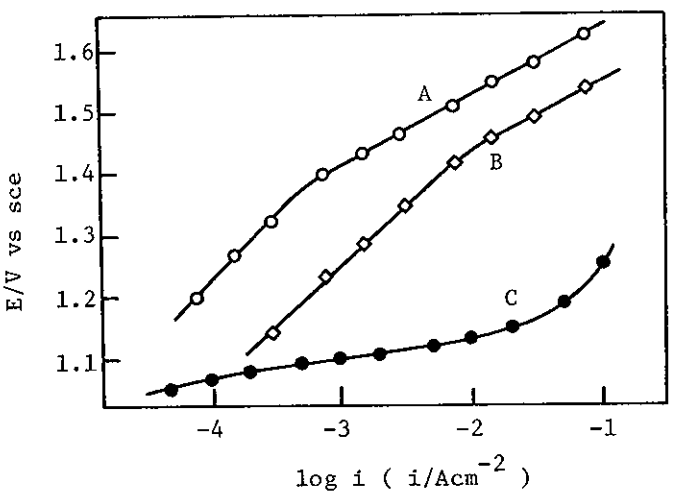

Fig. 23. Current-potential curves in 3M NaCl.
A: electrode A, B: electrode B, C: Pt/MnOx.

containing 3M NaCl was compared with the anodic oxidation of bromide ion on the massive Mn oxide electrodes. Figure 24 shows the polarization curves for the chlorine evolution together with those for the oxygen evolution. The chlorine evolution reaction was experimentally confirmed to be proceeding with the current efficiency of approximately 100% on each electrode in the mixed solution of 3M NaCl and 0.5M H_2SO_4. But, the

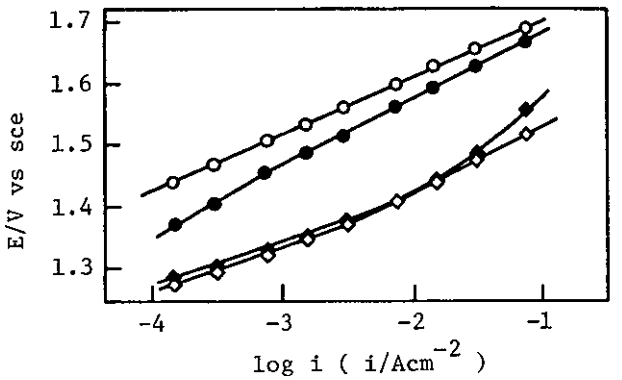

Fig. 24. Current-potential curves in 3M NaCl + 0.5M H_2SO_4 (closed symbols) and 0.5M H_2SO_4 (open symbols). ○,●: electrode A, ◇,◆: electrode B.

polarization curve of electrode B for the chlorine evolution is agreement with that for the oxygen evolution, and the somewhat similar result was obtained for electrode A. In the case of the latter electrode, the composition of the oxide, shown in Table 6, is reflected on the polarization curve. It is, therefore, considered that the rate-determining step in the chlorine evolution reaction is actually identical with that in the oxygen evolution reaction on the massive Mn oxide electrodes. This means the process of oxygen and chlorine evolution through a common stage. For the oxidation of bromide ion, however, the Mn oxide electrodes exhibit the normal behaviour observed on metal electrodes [63], as shown in Fig. 25. This difference in anodic behaviour seems to result from the redox potentials of Cl^-/Cl_2 and Br^-/Br_2. Bromide ion adsorbs on the surface of the Mn oxides and then discharges with the normal mechanism, whereas the charge transfer from chloride ion can occur only after the oxidation of the electrode surface because the

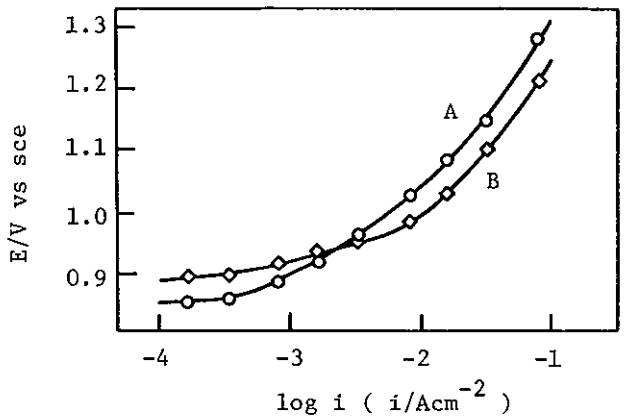

Fig. 25. Current-potential curves in 2M KBr + 0.5M H_2SO_4.
A: electrode A, B: electrode B.

oxidation potential of chloride ion seems to be higher than that of the electrode surface itself.

In order to support the above speculation, the reaction orders of various species were determined for oxygen and chlorine evolution reactions on the Mn oxide electrodes and the reaction mechanisms are discussed. The reaction orders were estimated by the dependency of the current densities at constant potentials on the activities of the reactive species in the solution.

Table 8. Summary of reaction orders for O_2 and Cl_2 evolution.

Electrolyte		Reaction order (log i/ log a_j)		Reaction
		A	B	
$H_2SO_4 + K_2SO_4$	low η	0.1	1.0	O_2
($j = H^+$)	high η	0.1	0.1	
KOH		0.9	0.9	
($j = OH^-$)				
NaCl		0	0	Cl_2
($j = Cl^-$)				
NaCl + HCl		0	0	
($j = H^+$)				

The results are shown in Table 8 with respect to each electrode. For the reaction of anodic oxygen evolution, the reaction orders of H^+ ion in the acidic solution and OH^- ion in the alkaline solution are approximately zero and unity, respectively, except for the low overvoltage region on electrode B where the participation of the cathodic process can not be ignored. These data for oxygen evolution reaction are practically in agreement with those on the film-type electrodes. On the other hand, unusual data were obtained for the chlorine evolution reaction on the massive Mn oxide electrodes. In general, the reaction order with respect to Cl^- ion in the anodic evolution of chlorine is 1 or 2 on usual metal and metal oxide electrodes [7, 64], and the current density is also dependent on the pH of the electrolyte, especially at metal oxide electrodes [18]. However, the present results show that on the massive Mn oxide electrodes the reaction rate of the anodic chlorine evolution is independent on the activities of not only proton but also chloride ion. Such results with respect to the reaction orders and the anodic polarization characteristics provide the following suggestions; Even in the anodic evolution of chlorine, the rate-controlling step is the same one as in the oxygen evolution, which is probably the first charge transfer step involving the H_2O molecule or the OH^- ion.

According to the model of the metal oxide-solution interface proposed by Ahmed and Maksimov [65], the surface of the Mn oxide in the acidic solution is represented by the forms such as

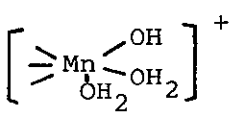

It is considered that the charge transfer process, or common rate-determining step both for oxygen and chlorine evolution, is expressed by the oxidation process of the central metal cation, $Mn^{(z)}$,

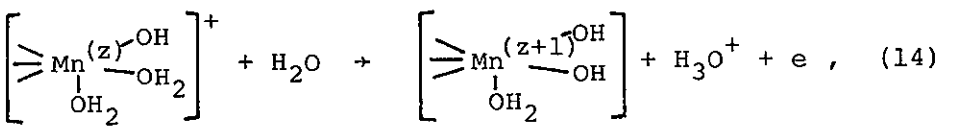

$$+ H_2O \rightarrow + H_3O^+ + e \ , \quad (14)$$

where z represents the valency of the manganese. Though the value of z is undefined, the active site is probably one formed from the Mn(III) for both reactions. Even on electrode A, whose bulk composition is β-MnO_2, the Mn(III) sites may be produced at the oxide surface by the formation of oxygen vacancy during the electrode preparation [66]. The high activity of the Mn(III) site may be similar to that of the Ir(III) site in the anodic oxide film of the Ir electrode reported by Gottesfeld and Srinivasan [67]. They have pointed out that high activities might be exhibibited by metastable states of the oxide catalyst associated with intermediate oxidation states.

Although, in this work, no informations were obtained on the subsequent processes yielding finally O_2 and/or Cl_2 and regenerating the site $Mn^{(z)}$, one of the presumable following step is a catalytic cycle such as sheme (15), since the evolution reactions of both oxygen and chlorine take place via a common process.

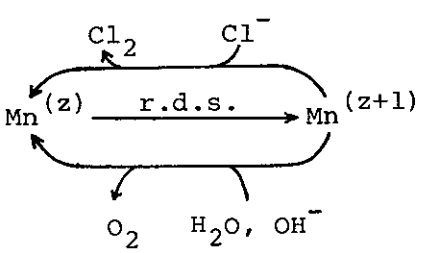

(15)

Consequently, the H_2O molecule, the OH^- ion or the Cl^- ion may be oxidized to the oxygen and the chlorine,respectively, by the Mn in the high oxidation state, $Mn^{(z+1)}$, which is probably the Mn(IV) at the surface, and then the $Mn^{(z+1)}$ may be reduced to the initial low oxidation state, $Mn^{(z)}$. The somewhat similar mechanism with the valence change of oxide surface during the electrode reaction has been first proposed by Yeager et al [24] for the anodic evolution of oxygen on the DSA-type RuO_2 electrode in alkaline solutions and accepted by Srinivasan et al [68] for the same reaction on NiOx, $NiCo_2O_4$ and RuO_2/TiO_2 electrodes.

The reason for such unique characteristics of Mn oxide electrodes can be related to the high reactivities of Mn oxides and the redox potential of Mn(III)/Mn(IV) (E_o = 0.98V vs nhe for Mn_2O_3/MnO_2) which is fairly near those of Cl^-/Cl_2 and H_2O/O_2. Further details of the differences in the polarization characteristics between the massive Mn oxides and the film-type electrodes will be discussed in the next chapter.

4. SUMMARY

The anodic characteristics of the massive manganese oxides were investigated in aqueous solutions. The results obtained in this chapter are summarized as follows.

1. The thermal treatment of the massive β-MnO_2 at 480°C or above leads to the formation of α-Mn_2O_3, and the redox reaction of Mn(III)/Mn(IV) accompanied by the diffusion of the H^+ ion

was characterized in the solid phase of the oxides.

2. The relatively high activity was observed for the anodic evolution of oxygen on the mixed oxide of β-MnO_2 and α-Mn_2O_3, and the active site of the reaction was regarded as the Mn(III) site at the oxide surface.

3. It was suggested that the oxidation process of the Mn(III) site at the electrode surface is a common rate-determining step in both the oxygen and chlorine evolution on the massive manganese oxide electrodes.

CHAPTER 3

THE ANODIC CHARACTERISTICS OF THE MASSIVE β-MnO_2 DOPED WITH NOBLE METALS IN SODIUM CHLORIDE SOLUTION

1. INTRODUCTION

As shown in the previous chapter, the difference in characteristics is observed for the anodic evolution of chlorine between the massive manganese oxides and the film-type manganese oxides. It is most probable that incorporation of noble metals into the manganese oxides occurs slightly in the film-type electrodes, because the noble metals such as Ru and Pt are used as an intermediate layer and a substrate, respectively. Most of noble metals and their oxides exhibit high catalytic activity for the anodic evolution of chlorine [4-22]. Therefore, it seems possible that the presence of small amounts of noble metals in the massive manganese oxides affects their polarization characteristics in NaCl solution.

In this chapter, in order to evaluate above supposition, the massive manganese oxides were doped with a slight amount of noble metals and then their anodic characteristics were investigated mainly in 3M NaCl. Furthermore, the role of doped metals was discussed.

2. EXPERIMENTAL

The massive manganese oxides were prepared by the same procedure as that described in chapter 2. Foreign metals were doped in the massive manganese oxides by using mixed aqueous solution of 50vol.% $Mn(NO_3)_2$ and 0.1M chlorides of foreign metals (or metal salts) containing HCl as the original solutions for thermal decomposition. The temperature of the thermal decomposition was controlled at 160 - 180°C, and all of the resulting oxides were thermally treated at 450°C for 20h. The starting raw materials used and the predicted valences of the doped foreign metals are summarized in Table 9. To avoid complexity, the test electrodes of this type will be referred to as MnO_2-M(C), where C represents the concentration of the doped metal, M, in at.% M/Mn. The maximum concentration of the doped metals was fixed to 2at.%.

The X-ray diffraction patterns of all test electrodes exhibited that of pure β-MnO_2 and no patterns assigned to the metals or their oxides doped in β-MnO_2 were observed in any

Table 9. Summary of doped metals

Doped metal	Raw material	Predicted valency in β-MnO_2
Pd	$PdCl_2$	Pd(II) or Pd(0)
Pt	H_2PtCl_6	Pt(II) or Pt(0)
Ru	$RuCl_3$	Ru(IV)
Ir	$IrCl_4$	Ir(IV)
Rh	$RhCl_3$	Rh(III)
Ti	$TiCl_3$	Ti(IV)
V	NH_4VO_3	V(V)
Mn	$MnCl_2$	Mn(III)

cases.

Most of electrochemical measurements were performed in aqueous solutions of 0.5M H_2SO_4 and 3M NaCl at 30°C. The electrolytic solutions were prepared from the special grade reagents and twice-distilled water, and were purified by electrolysis over 40h before use. The current-potential curves were galvanostatically measured under the conditions of N_2 gas bubbling in electrolytic solutions in order to eliminate dissolved oxygen and to minimize the concentration overvoltages. The ohmic drop was determined by the current interrupting method. The ac impedance measurements were carried out at equilibrium potential in the Cl_2-saturated 3M NaCl solution (P_{Cl_2} = 1atm).

3. RESULTS AND DISCUSSION

Figure 26 shows the current-potential curves obtained on the MnO_2-Ru(0.5), MnO_2-Ru(1) and MnO_2-Ru(2) electrodes in 3M NaCl, compared with those on the pure β-MnO_2 and Ti/RuOx/MnOx electrodes. At current densities higher than about 10mA/cm^2, slight bendings of the curves due to concentration polarization are observed. However, it was experimentally confirmed by using rotating disk electrodes that high overvoltage observed at the pure β-MnO_2 electrode cannot be attributed to concentration overvoltage only. The chlorine overvoltage as well as the Tafel slope decreases with the increase in concentration of doped Ru. The curve of the film-type electrode, Ti/RuOx/MnOx,

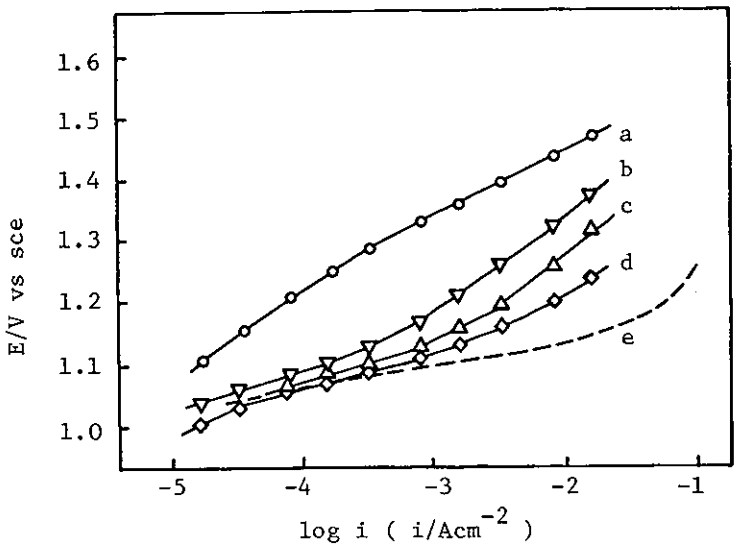

Fig. 26. Current-potential curves of metal-doped electrodes in 3M NaCl.
a:pure β-MnO_2, b:MnO_2-Ru(0.5), c:MnO_2-Ru(1), d:MnO_2-Ru(2), e:Ti/RuOx/MnOx.

is appreciably similar to that of the MnO_2-Ru(2) electrode: such similarity may suggest that the RuOx used as an intermediate layer in the Ti/RuOx/MnOx electrode migrates in part to the surface MnOx layer to form Ru-doped Mn oxide.

Figure 27 shows the current-potential curves of MnO_2 electrodes doped with 2at.% of different metals. It is obvious from this figure that Ru, Ir, Pt and Pd affect the chlorine overvoltage in a striking manner. Rh revealed little doping effect and both Ti and V exhibited no effects on the chlorine evolution reaction. Furthermore, it is evident that chloride ion contained in the original solutions for electrode preparation is not responsible for the variation in anodic characteristics, because the current-potential curve observed on the MnO_2-Mn(2) electrode is approximately in agreement with the curve on the

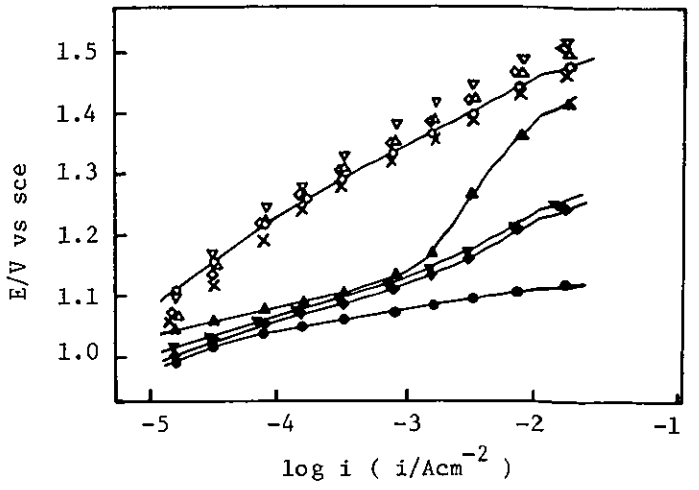

Fig. 27. Current potential curves of metal-doped electrodes in 3M NaCl.
○:pure β-MnO_2, ×:MnO_2-Mn(2), △:MnO_2-Ti(2)
▽:MnO_2-V(2), ◇:MnO_2-Rh(2), ▲:MnO_2-Pt(2)
▼:MnO_2-Ir(2), ◆:MnO_2-Ru(2), ●:MnO_2-Pd(2).

pure β-MnO_2 electrode. Therefore, these doping effects may reflect the catalytic activity for the chlorine evolution reaction of the doped metals or their oxides. The most effective dopant of all studied was Pd. In fact, the Pd metal or PdO possesses extremely high activity for the anodic evolution of chlorine [69].

In order to evaluate the doping effects on the oxygen evolution reaction, the current-potential curves of various electrodes were measured in 0.5M H_2SO_4, and the results are shown in Fig. 28. Any significant effects on the oxygen evolution reaction were not observed on all electrodes examined. Such difference in doping effects between the chlorine and oxygen evolution reactions seems to be attributable to the difference in catalytic activities of β-MnO_2 itself for those

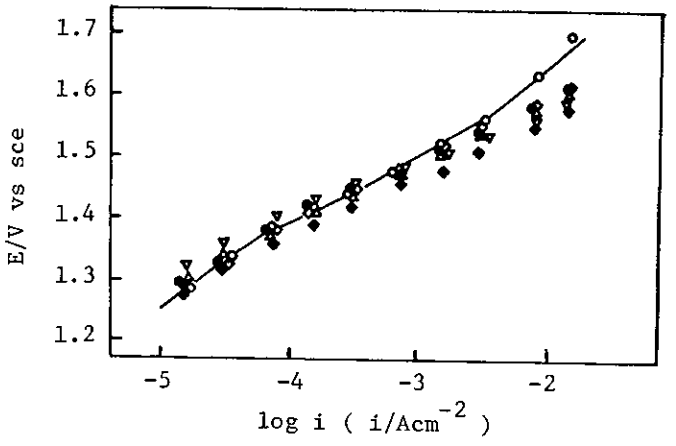

Fig. 28. Current-potential curves of metal-doped electrodes in 0.5M H_2SO_4.
○ : pure β-MnO_2, ● : MnO_2-Pd(2), ◇ : MnO_2-Ru(2)
◆ : MnO_2-Rh(2), △ : MnO_2-Ir(2), ▽ : MnO_2-Pt(2).

two reactions. For the oxygen evolution reaction, the catalytic activity of β-MnO_2 is as high as those of the doped metals. Therefore, the significant doping effects can not be revealed in the β-MnO_2 doped with the noble metals. On the other hand, the doped metals act effectively for the chlorine evolution reaction because of the relatively low activity of β-MnO_2 itself for that reaction.

Figure 29 shows variation of electrode potentials with time under the galvanostatic polarization at 5mA/cm^2 in 3M NaCl. The anodic shift of electrode potentials was observed at any electrodes within the first one hour, but it became negligible after that. Though the iR drops in the electrode potentials were corrected for the respective electrodes, the concentration overvoltages, which might be different in every electrode, are involved in the figure. Even after these experiments, the

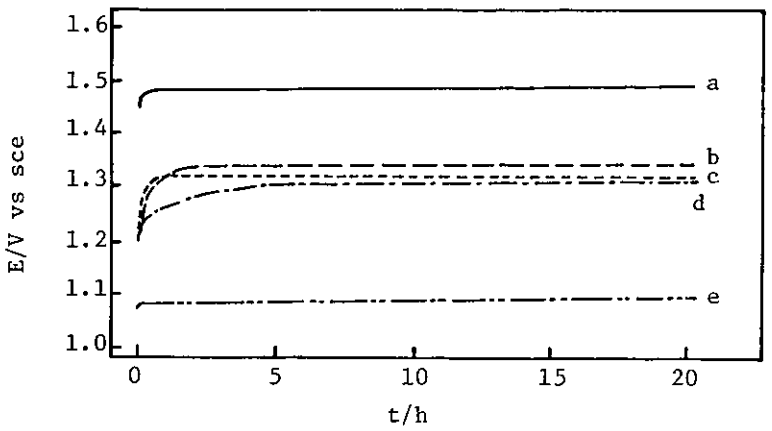

Fig. 29. Potential-time curves of metal-doped electrodes at 5mA/cm^2 in 3M NaCl.
a:pure β-MnO_2, b:MnO_2-Ir(2), c:MnO_2-Ru(2), d:MnO_2-Pt(2), e:MnO_2-Pd(2).

current-potential curves could be well-reproduced for all electrodes. Furthermore, no changes of the electrode surfaces were observed in their appearances. These results suggest that the anodic currents, shown in Fig. 27, are entirely due to the anodic evolution of chlorine but not to the anodic dissolution of doped metals.

In order to elucidate the role of the doped metals, the metal-adsorbed MnO_2 electrodes, MnO_2/M^x(ad), were prepared and their polarization characteristics were measured in 3M NaCl solution. The adsorption of noble metals on the pure β-MnO_2 electrodes were performed by soaking the pure β-MnO_2 electrode in 10^{-2}M solutions of noble metal chloride containing 2% HCl for 50h, followed by washing with deionized water for 10min to remove ions adhered physically on the oxide surface. The current-potential curves on metal-adsorbed electrodes are shown

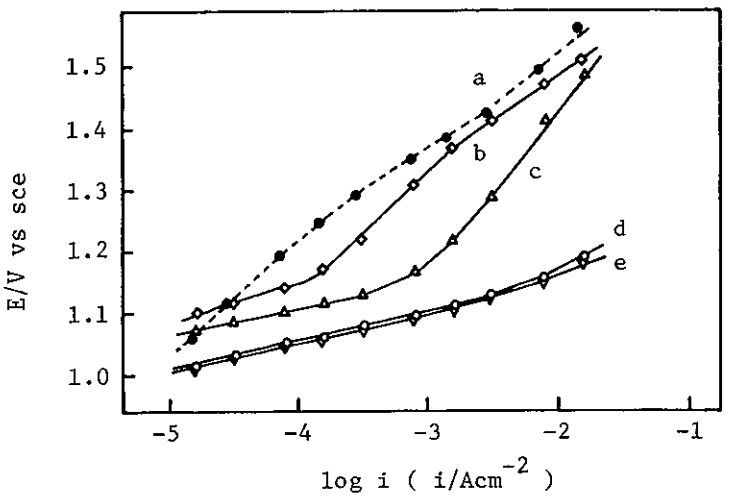

Fig. 30. Current-potential curves of metal-adsorbed electrodes in 3M NaCl.
a:pure β-MnO_2, b:MnO_2/Rh^{III}(ad), c:MnO_2/Pt^{IV}(ad), d:MnO_2/Pd^{II}(ad), e:MnO_2/Ru^{III}(ad).

in Fig. 30. The MnO_2/Pd^{II}(ad) electrode exhibits considerably high activity comparable to that of the MnO_2-Pd(2) electrode. Besides Pd(II), Pt(IV) as well as Ru(III) also in this type of electrode contribute to the decrease in chlorine overvoltages. On the MnO_2/Rh^{III}(ad) electrode, the effect of Rh(III) is hardly detected, quite the same as in the case of the MnO_2-Rh(2) electrode. These noble metal chlorides are considered to exist as chlorocomplexes in the dilute solutions of hydrochloric acid [70]. When β-MnO_2 is soaked in the chloride solution, the chlorocomplex of noble metal cation is presumed to be adsorbed on the surface of β-MnO_2 accompanied by the surface ion exchange (or the surface chelation) analogously to the case of adsorption of $ZnCl_4^{--}$ on the MnO_2 powder [71]. For example, it can be speculated that the Pd(II) ion is attached on the

surface of the β-MnO_2 in the following manner:

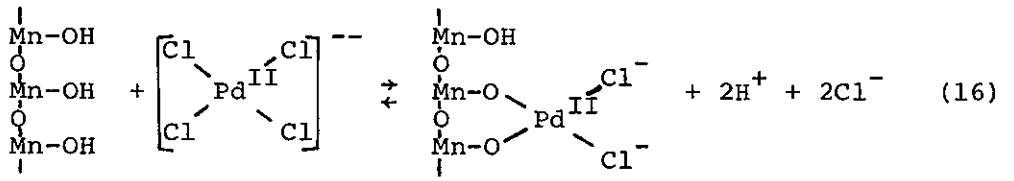

(16)

The potential-time curves on the metal-adsorbed electrodes are shown in Fig. 31. On the MnO_2/Pt^{IV}(ad) electrode the potential shifted to more anodic than 1.4V within several tens of minutes after the start of polarization, while much longer duration was consumed to increase overvoltages on the $MnO_2/Pd^{II}_{(ad)}$ and MnO_2/Ru^{III}(ad) electrodes. These anodic shifts in the potentials are due to the desorption of noble metals and the difference in the time required to shift up may be associated with the tightness of the adsorption of each metal. Therefore, the lower overvoltages in initial periods are caused by the

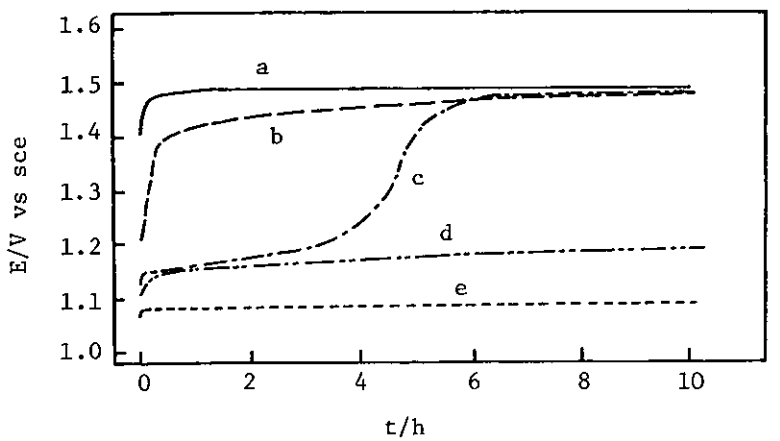

Fig. 31. Potential-time curves of metal-adsorbed electrodes at 5mA/cm^2 in 3M NaCl.
a:pure β-MnO_2, b:MnO_2/Pt^{IV}(ad), c:MnO_2/Pd^{II}(ad), d:MnO_2/Ru^{III}(ad), e:metal-doped electrode(MnO_2-Pd(2)).

high activities of adsorbed metals for the chlorine evolution reaction.

From the fact that the metal-adsorbed electrodes behave like the metal-doped electrodes, it is considered that even in the case of the metal-doped electrodes noble metal sites exposed at the surface only serve effectively, rather than that the doping effects are resulted from the variation in bulk properties (electronic and/or structural) of β-MnO_2 by doping of noble metals.

The role of doped metals was considered on the basis of Tafel slope (b) and exchange current density (i_0). The Tafel slopes for the anodic evolution of chlorine on the metal-doped electrodes were determined in the low overvoltage region where the concentration polarization could be neglected. The values obtained are summarized in Table 10, in which the data for the corresponding metals (Pd and Pt) and the metal oxides (PdO, PtO_2, RuO_2 and IrO_2) are included. For the chlorine evolution reaction at low overvoltage, two well-known mechanisms have been accepted in general, ie,

Table 10. Tafel slope for the anodic evolution of chlorine

Metal-doped electrode	b(V/dec)	Metal	b(V/dec)	Metal oxide	b(V/dec)
MnO_2-Pd(2)	0.033	Pd	0.033	PdO	0.030
MnO_2-Pt(2)	0.045	Pt	0.042*	PtO_2	0.03[RT/2F]**
MnO_2-Ru(2)	0.055			RuO_2	0.04[2RT/3F]**
MnO_2-Ir(2)	0.057			IrO_2	0.04[2RT/3F]**

* Reference[72]
** Reference[18,20]

$$Cl^- \rightleftarrows Cl\bullet + e$$

$$2Cl\bullet \rightarrow Cl_2 \qquad \text{(r.d.s.)} \qquad (17)$$

and

$$Cl^- \rightleftarrows Cl\bullet + e$$

$$Cl\bullet + Cl^- \rightarrow Cl_2 + e \qquad \text{(r.d.s.)} \; . \qquad (18)$$

For the mechanisms (17) and (18), one can obtain the theoretical Tafel slopes of 0.03V (RT/2F) and 0.04V (2RT/3F), respectively. It is evident that the chlorine evolution reaction on the MnO_2-Pd(2) electrode proceeds by the mechanism (17), just as on the metal Pd and PdO electrodes. The reaction on the MnO_2-Pt(2) electrode proceeds through the mechanism (18) like on the metal Pt electrode. On the other hand, the values of Tafel slope observed on the MnO_2-Ru(2) and MnO_2-Ir(2) electrodes are larger than that on the MnO_2-Pd(2) electrode. This tendency seems to be in agreement with that in the pure oxide electrodes ($RuO_2 \simeq IrO_2$ > PdO in Tafel slopes), though each value on the metal-doped electrode does not exactly correspond to that on the pure oxide electrode. Roughly speaking, the mechanism of the chlorine evolution reaction on the noble metal-doped electrode reflects each mechanism on the doped metal or metal oxide electrode.

The exchange current densities, i_0, for the chlorine electrode reaction on metal-doped electrodes are given in Table 3, compared with that on the smooth Pt electrode. The

Table 11. Exchange current density for the chlorine electrode reaction

Electrode	i_o (A/cm^2)
MnO_2-Pt(2)	6.8×10^{-2}
MnO_2-Pd(2)	6.1×10^{-2}
MnO_2-Ru(2)	4.1×10^{-2}
MnO_2-Ir(2)	3.8×10^{-2}
smooth Pt	6.7×10^{-3}

i_0 values were calculated from the charge-transfer resistance, θ, by using the following equation

$$i_0 = \frac{RT}{2F\theta} . \qquad (19)$$

The θ values were determined by Sluyters' method [73] from the ac impedance measured at the reversible potential (3M NaCl, P_{Cl_2} = latm). The i_0 values shown in Table 11 are reasonable in magnitudes if the roughness of the electrode surface is taken into account. Since these oxides were prepared and pretreated entirely in the same conditions, their true surface areas can be considered to be approximately the same as each other, except for the case of the smooth Pt electrode. The i_0 on the MnO_2-Pt(2) and the MnO_2-Pd(2) electrodes are somewhat larger than those on the MnO_2-Ru(2) and the MnO_2-Ir(2) electrodes. This result seems to be compatible with the tendency of the pure oxides of noble metals where the order of i_0 has been reported as $PtO_2 \gtrsim PdO > RuO_2 \simeq IrO_2$ [18,69].

From the above discussions on the reaction mechanisms and the order of the exchange current densities, it is presumed that the chlorine evolution reaction on the noble metal-doped

electrodes proceed on the sites of doped metals or their oxides. However, other dopants such as Ti, V and Rh did not contribute to activation of β-MnO_2 for the chlorine evolution reaction. Probably this is because: (1) the dopant is not effectively dispersed on the electrode surface; or (2) the activity of the doped metal itself is comparable to or lower than that of the β-MnO_2. The second reason is more probable.

The current-potential curve on the MnO_2-Pd(2) electrode is compared with that on the PdO electrode in Fig. 32. The PdO electrode used was prepared by thermally decomposing $PdCl_2$ at 650°C in O_2 atmosphere for 3h, followed by binding PdO powder with Teflon resin (15wt.%). If the doped Pd exist in MnO_2 as physical mixture, one can expect that the current density observed at the MnO_2-Pd(2) electrode is equal to 2% of that at the PdO electrode. However, it is clear from Fig. 32 that this is not the case.

There seems to be an activation effect or a synergistic

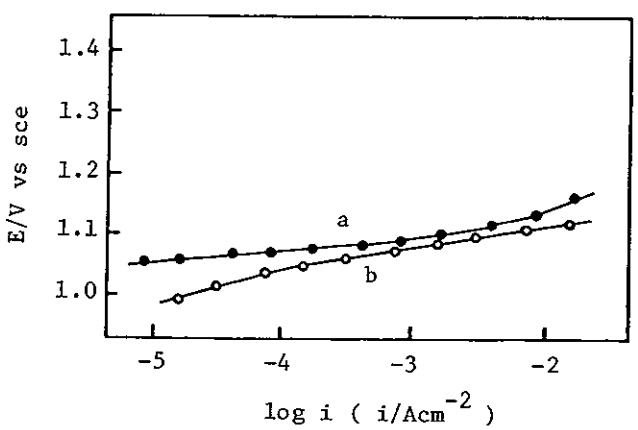

Fig. 32. Current-potential curves in 3M NaCl.
a:pure PdO, b:MnO_2-Pd(2).

effect produced by mixing of the catalysts in the MnO_2-Pd system. This attractive phenomenon might be analogous to that observed on the SnO_2-Pt system [74,75] or on the Pt doped tungsten bronze electrode [76,77]. Accordingly, further details in the mixed Mn-Pd oxide system will be discussed in the next chapter.

4. SUMMARY

The anodic characteristics of the massive β-MnO_2 doped with noble metals were studied in sodium chloride solution and the results obtained are summarized as follows.

1. The doping of noble metal, especially Pd, decreases the chlorine overvoltage enomously, whereas it scarcely affects the oxygen evolution reaction.

2. The similarity of the polarization characteristics of the doped electrodes to those of the metal-adsorbed electrodes suggests the significance of the noble metal sites exposed at the surface.

3. The data of the Tafel slopes and the exchange current densities also support that the noble metal sites serve as an active site for the chlorine evolution reaction.

CHAPTER 4

THE ELECTROCATALYTIC ACTIVITIES OF THE MIXED Mn-Pd OXIDES FOR THE CHLORINE EVOLUTION REACTION

1. INTRODUCTION

Electrocatalysis of metal oxides doped with small amounts of foreign metals has become of interest in recent years. There have been many studies, for example, the cathodic reduction of oxygen on the Pt-doped Na_xWO_3 [76,77] and the anodic evolution of oxygen and chlorine on the Ru-doped SnO_2 [75,78] or Co_3O_4 [79]. Besides these, it was found in chapter 3 that MnO_2 doped with the noble metals, especially Pd, exhibits a very high activity for the anodic evolution of chlorine. It was also reported that the addition of MnO_2 in the noble metal oxides or their mixed oxides decreased the oxygen overvoltage [80] and improved the anodic durability in chlorate/chloride solution [81].

Though the active sites for the electrochemical reactions on these doped (or mixed) electrodes were supposed to be the noble metal sites, the mechanism of the activation by doping (or mixing) has been still ambiguous. Therefore, in this chapter, the electrocatalytic activity of the Pd-doped massive MnO_2 was examined for the chlorine evolution reaction in order to characterize the base metal oxides doped with noble metals more definitly. Furthermore, the anodic polarization characteristics of the film-type electrodes of mixed Mn-Pd oxides

were investigated in a sodium chloride solution, in a view of application to the practical electrolysis.

2. EXPERIMENTAL

The massive MnO_2 electrodes doped with Pd were prepared by the same procedure as that described in chapter 3, and will be referred to as MnO_2-Pd(C_{Pd}), where C_{Pd} represents the concentration of doped Pd in at.% Pd/Mn ($0.2 \leqq C_{Pd} \leqq 5$). The X-ray diffraction patterns of the massive electrodes exhibited only that of β-MnO_2 phase and no pattern assigned to Pd or PdO was observed in any case. A pure PdO electrode made of Teflon-bonded PdO powder was also used as a test electrode for comparison. These test electrodes were polished with emery papers to present the same condition of the working surface.

The film-type electrodes were prepared by the thermal decomposition method as shown in chapter 1. A titanium plate (10 x 10 x 0.5mm) was used as a substrate. Required amounts of aqueous solutions of $Mn(NO_3)_2$, $PdCl_2$ and $RuCl_3$ were mixed together and then applied to one side of the substrate. The thermal decomposition was carried out at 450°C in air. The amounts of oxide loadings in the film-type electrodes will be indicated by the value in parentheses in mol of metal/cm^2 for each electrode.

Most of electrochemical measurements were performed by the same procedures as those described in the previous chapters. The anodic current-potential curves for the chlorine evolution

were measured in 3M NaCl or 1M $HClO_4$ + 3M NaCl under the galvanostatic condition. Stirring of the electrolytic solution and elimination of dissolved gases were accomplished by a continuous bubbling of N_2. The cathodic current-potential curves for the chlorine reduction were obtained potentiostatically in 1M $HClO_4$ saturated with latm Cl_2. These polarization measurements were performed at 30°C. The current densities calculated from the charge transfer resistances in the Faraday impedance [21,73] were used as those for Arrhenius plots to obtain the apparent activation energies. All of current densities shown in this work will be indicated by the apparent one based on the geometric area ($1cm^2$).

3. RESULTS AND DISCUSSION

1. Electrocatalytic activity of the massive MnO_2-Pd electrode

Figure 33 shows the anodic current-potential curves of the MnO_2-Pd electrodes in 3M NaCl + 1M $HClO_4$. An anodic Tafel slope, b_a, of 0.03V was observed on the highly doped electrodes (C_{Pd} = 2 and 5). On the other hand, the curves obtained on the lower Pd-content electrodes had not well-defined Tafel regions. The steep bending of the curves shown in the more anodic region seems to be attributable to change in the surface coverage by the reaction intermediate rather than to contribution of the concentration polarization as reported for the Pt electrode [82]. This will be further discussed in the

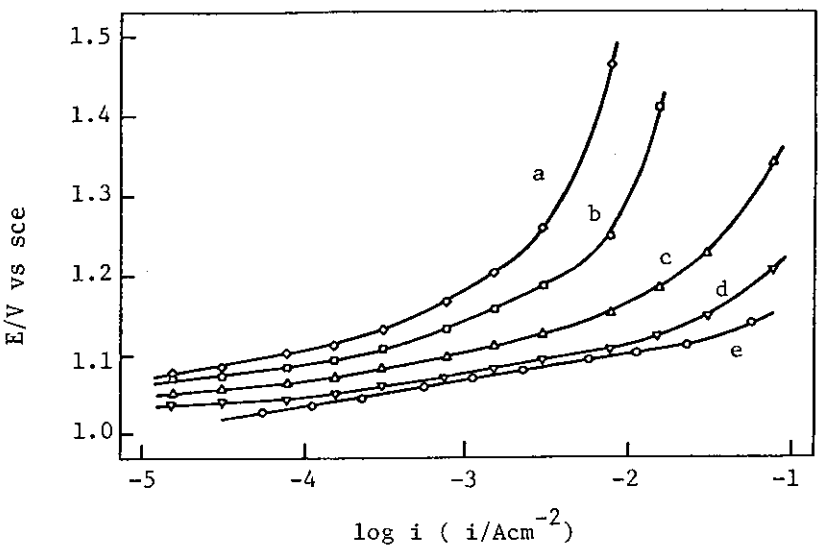

Fig. 33. Current-potential curves of MnO_2-Pd(C_{Pd}) electrodes in 3M NaCl + 1M $HClO_4$.
C_{Pd} = 0.2(a), 0.5(b), 1(c), 2(d) and 5(e).

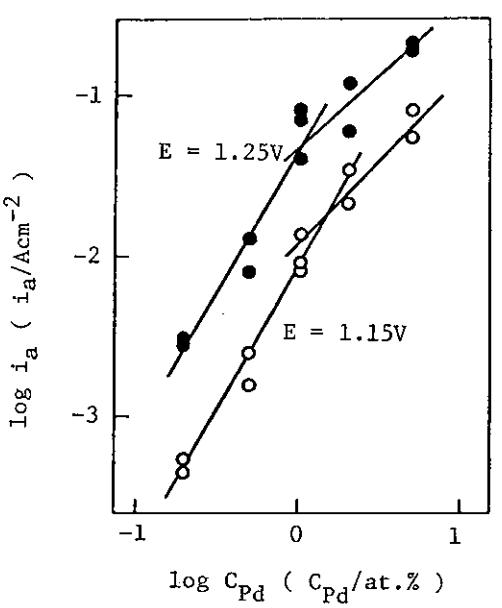

Fig. 34. log i_a *vs* log C_{Pd} plots obtained from current-potential curves.

later part of this section.

Based on the data of Fig. 33, the current densities, i_a, at E = 1.15V and E = 1.25V are plotted in Fig. 34 against the concentration of doped Pd, C_{Pd}. More than two samples were examined for each C_{Pd} to confirm the reproducibility. Some variance is detectable in the figure, suggesting that the C_{Pd} in the oxide bulk does not closely reflect the concentration of Pd at the electrode surface, but, as a whole, log i_a increases with increasing log C_{Pd}. The current density, or the catalytic activity, tends to saturate in the high C_{Pd} region. The slopes of the lines shown in Fig. 34 are 1.8 and 1.0 at low C_{Pd} and high C_{Pd}, respectively.

Figure 35 shows the cathodic current-potential curves in 1M $HClO_4$. The oxide itself (MnO_2 and/or PdOx) is scarcely reduced in this potential region as shown by curve (f) in the figure. The cathodic limiting currents in curves (a) - (e)

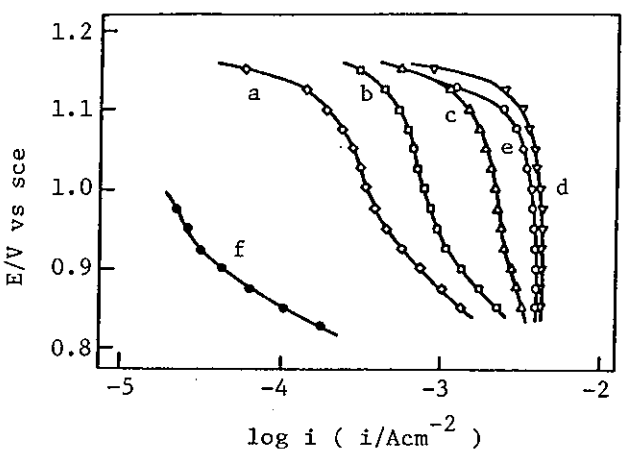

Fig. 35. Current-potential curves of MnO_2-Pd(C_{Pd}) electrodes in Cl_2-saturated 1M $HClO_4$ (a-e) and in N_2-saturated 1M $HClO_4$ (f).
C_{Pd} = 0.2(a), 0.5(b), 1(c), 2(d) and 5(e,f).

suggest that the chlorine reduction reaction on these electrodes is controlled by the step of the dissociative adsorption of chlorine. It is considered that the bending of the curves at more cathodic potential, especially on the low C_{Pd}-electrodes, is due to somewhat contribution of the reduction current of the oxide itself or to overapping of the chlorine reduction on the MnO_2.

The plots of log i_c vs log C_{Pd} are shown in Fig. 36 based on the data of Fig. 35. In the high C_{Pd} region, log i_c tends to saturate with increasing log C_{Pd} while the relation between i_c and C_{Pd} in the low C_{Pd} region is approximately of first-order. It is apparent from this figure that the dissociative adsorption of chlorine takes place at the Pd site preferentially. If the cathodic limiting current reflects the number of the Pd sites at the electrode surface, Fig. 36 indicates the relation

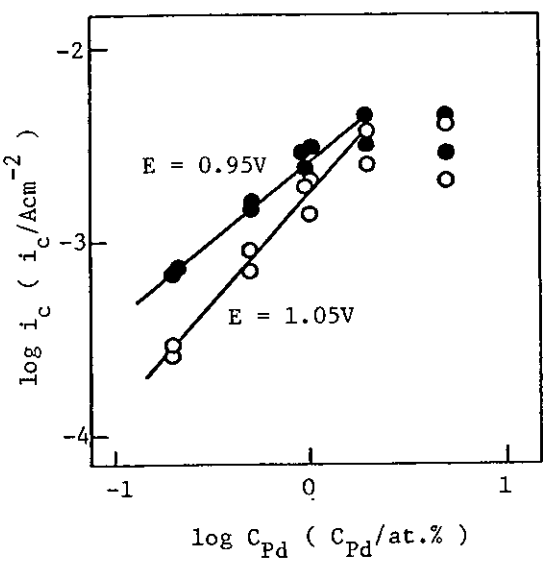

Fig. 36. log i_c *vs* log C_{Pd} plots obtained from current-potential curves.

between the bulk concentration of the doped Pd (C_{Pd}) and the number of the effective sites for the chlorine electrode reaction within the exposed Pd sites at the electrode surface (i_c). Figure 37 shows the plot of log i_a (at E = 1.15V in Fig. 34) vs log i_c (at E = 1.05V in Fig. 36) for all electrodes examined. A good linear relation with a slope of 2.0 is detectable not only in the low C_{Pd} (ie low i_c) region but also in the high C_{Pd} (ie high i_c) region, in contrast to the relations shown in Figs. 34 and 36. The linearity of the data in Fig. 37 suggests that the saturation of the current densities in the high C_{Pd} region observed in Figs. 34 and 36 is caused by the non-linear relation between the number of the effective Pd sites at the

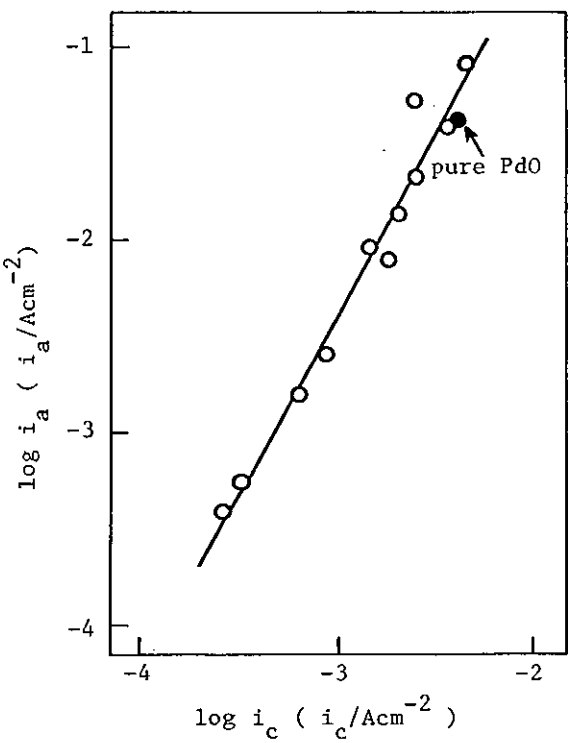

Fig. 37. log i_a *vs* log i_c plot obtained from Figs. 34 and 36.

surface and the Pd concentration in the oxide bulk. The absolute number of the Pd sites exposed at the surface was not measured directly. But it must be proportional to the bulk concentration of the doped Pd, because any result suggesting heterogeneity of the doped Pd in the oxide was not obtained. That is, it was confirmed that any significant dispersion of the data was not observed in the different electrode surfaces prepared by cutting off the massive samples with the emery papers. The saturation of the current densities observed in Figs. 34 and 36 eventually means that the fraction of the effective sites for participating in the chlorine electrode reaction decreases with increasing C_{Pd} within all the exposed Pd sites at the electrode surfaces.

From the results, $b_a = 0.03V$ and $b_c = -\infty$ at the relatively low overvoltages, as shown in Figs. 33 and 35, the chlorine electrode reaction on the MnO_2-Pd electrodes seems to proceed with so-called catalytic mechanism (Volmer-Tafel mechanism), equation (20) and (21),

$$Cl^- \rightleftharpoons Cl\bullet + e \qquad (20)$$

$$2Cl\bullet \leftrightarrow Cl_2 \qquad (21)$$

where equation (21) is the rate determining step. For the anodic reaction, the current density can be expressed by equation (22),

$$i_a = k_a[Cl\bullet]^2 \qquad (22)$$

where [Cl•] is the concentration of the reaction intermediate,

$Cl^{\bullet}$, per unit surface area, and is a function of the electrode potential, E, the concentration of Cl^{-} ion in the electrolyte, C_{Cl^-}, the number of the available active sites, N_{Pd}, and the degree of their coverage with $Cl^{\bullet}$, $\theta_{Cl^{\bullet}}$. If C_{Pd} is altered under a condition of constant E and C_{Cl^-}, $[Cl^{\bullet}]$ is given by

$$[Cl^{\bullet}] = \theta_{Cl^{\bullet}} N_{Pd} \quad , \tag{23}$$

and then equation (22) can be rewritten in equation (24),

$$i_a = k_a \theta_{Cl^{\bullet}}^2 N_{Pd}^2 \quad . \tag{24}$$

For the cathodic reaction,

$$i_c = k_c N_{Pd}/2 \quad . \tag{25}$$

From equations (24) and (25), it can be deduced that

$$i_a = k\theta_{Cl^{\bullet}}^2 i_c^2 \quad , \tag{26}$$

where $k = 4k_a/k_c^2$. By comparing equation (26) with the experimental result of $i_a \propto i_c^2$ shown in Fig. 37, it is proved that $\theta_{Cl^{\bullet}}$ is kept constant during the variation of C_{Pd}. Consequently, $\theta_{Cl^{\bullet}}$ is not defined for all Pd sites exposed at the surface but for the effective Pd sites for participating in the chlorine electrode reaction.

The proportionality between C_{Pd} and N_{Pd} in the low C_{Pd} region as shown in Fig. 36 indicates that the increase in the Pd content causes to increase the number of the active particles holding the particle diameter constant in the oxide [77]. This means that the active particles involving Pd are dispersed with microscopic homogeneity. If the area of the active

portion containing the Pd particles increases simply with C_{Pd} (or, if the doped Pd has a macroscopic structure as metal Pd or PdO), the relation of $i_a \propto C_{Pd}$ as well as $i_c \propto C_{Pd}$ should be observed experimentally. This is not the case. The results show that the increase in C_{Pd} leads to the increase in the number of the active sites per unit area on the atomic scale. The saturation of N_{Pd} in the high C_{Pd} region (in Fig. 35) seems to be attributable to that the dimensions of the active particles containing Pd grow with increase in C_{Pd} and that the particles become to have macroscopic structures as metal Pd or PdO. The relation between i_a and i_c on the tablet-type pure PdO electrode, which is also indicated in Fig. 37, is satisfied with the relation obtained on the MnO_2-Pd system. From the comparison of the reaction rate on the pure PdO electrode with that on the MnO_2-Pd electrode, it is assumed that the fraction of the uneffective sites for participating in the chlorine electrode reaction (the dead sites) is increased within all Pd sites at the surface even on the high C_{Pd}-electrodes as well as on the pure PdO electrode. The role of the MnO_2 as a support of the active catalyst, which is more significant in the low C_{Pd} region, is to disperse the Pd particles effectively on the atomic scale.

A typical dependence of the chlorine evolution reaction on the concentration of Cl^- ions is shown for the MnO_2-Pd(1) electrode in Fig. 38. Substantially analogous results were obtained on the other electrodes. By assuming the Langmuir adsorption isotherm one obtains

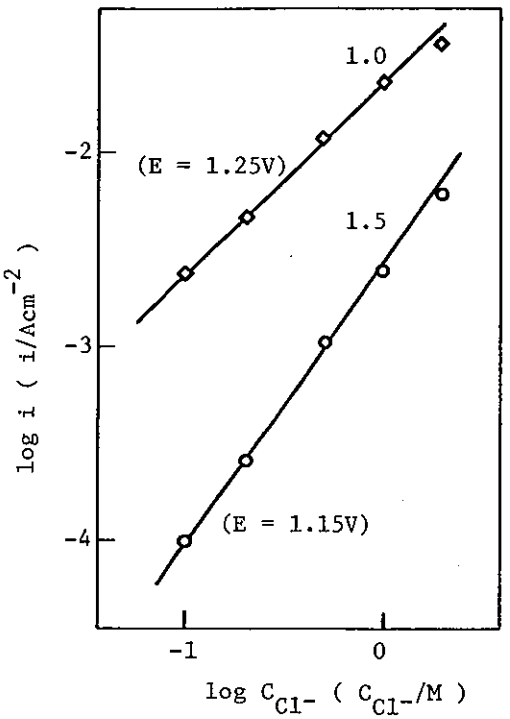

Fig. 38. Dependence of anodic current density on Cl^- ion concentration.

$$\theta_{Cl\bullet} = \frac{KC_{Cl^-}\exp(EF/RT)}{1 + KC_{Cl^-}\exp(EF/RT)} \tag{27}$$

where K is the quasi-equilibrium constant for equation (20). From equations (24) and (27),

$$i_a \propto \left[\frac{KC_{Cl^-}\exp(EF/RT)}{1 + KC_{Cl^-}\exp(EF/RT)}\right]^2 , \tag{28}$$

and then equation (28) can be replaced by equation (29) for convenience,

$$i_a \propto C_{Cl^-}{}^n \tag{29}$$

In this equation n is exactly equal to 2 for $\theta_{Cl\bullet} \to 0$ but it changes continuously from 2 to 0 with increasing $\theta_{Cl\bullet}$ (or E). The result shown in Fig. 38 means that the $\theta_{Cl\bullet}$'s have relatively large values at the measured potentials. The reaction order of 1.0 with respect to Cl^- ion at 1.25V can be also derived from the processes in which the primary Cl^- ion discharge step, equation (20), is rate-determining, but the retention of the relation of $i_a \propto [Cl\bullet]^2$ even at this potential (Fig. 34) strongly suggests that the recombination step, equation (21), is still rate-controlling.

Figure 39 shows the Arrhenius plots of the current densities for the chlorine evolution reaction. The apparent activation energies were calculated from the slopes of the straight lines in the figure and are summarized in Table 12. It is

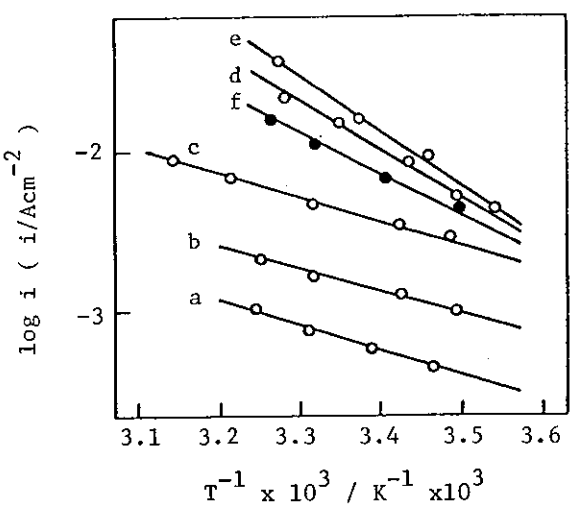

Fig. 39. Arrhenius plots for Cl_2 evolution on MnO_2-Pd(C_{Pd}) electrodes and pure PdO electrode.
C_{Pd} = 0.2(a), 0.5(b), 1(c), 2(d) and 5(e). pure PdO(f).

Table 12.
Apparent activation energy for the chlorine evolution reaction (E = 1.15V)

Electrode	Activation energy ($kj \cdot mol^{-1}$)
MnO_2-Pd(0.2)	31.9
(0.5)	26.8
(1)	29.3
(2)	57.3
(5)	66.9
Pure PdO	49.7

qualitatively proved that there is a difference in the activation energies between the low C_{Pd}-electrodes (C_{Pd} = 0.2, 0.5 and 1) and the high C_{Pd}-electrodes (C_{Pd} = 2 and 5). This distinction in the activation energies seems to correspond to the definite break in the log i_a vs log C_{Pd} plots shown in Fig. 34. An activation energy is one of the kinetic parameters in which any factor with respect to the real surface area of the electrode (or the number of active sites at the electrode) is not included, and it reflects the details of the reaction mechanism [83]. The relatively high values of the activation energies observed on the high C_{Pd}-electrodes are approximately equal to that on the pure PdO electrode, and then it suggests that on these electrodes not only the macroscopic reaction mechanisms but also the energy states of the reaction intermediates are similar to each other. On the other hand, the activation energies observed on the low C_{Pd} electrodes are relatively low. This result leads to the supposition that the energetic surroundings of the reaction intermediates on the low C_{Pd}-electrodes are appreciably different from that on the pure PdO electrode.

Because of the complexity of the electrode system, it is difficult to explain quantitatively the activation energy obtained on this type of electrode. However, the following qualitative concept may be present. On the MnO_2-Pd electrodes possessing low C_{Pd}, there are many Mn sites around the active Pd sites which are homogeneously dispersed on the atomic scale. The reaction rate of the primary Cl^- ion discharge step, equation (20), on the Mn site is considerably slower than on the Pd site. Thus the surface concentrations of Cl• on the low C_{Pd}-electrodes are held extremely low on the whole electrode surface, and are different from those on the high C_{Pd} or pure PdO electrode. The low values of the activation energy can be correlated with the instability in the state of the intermediate Cl•. As the Cl• on the Mn site is considered to be unstable, the process may involve a certain specific step such a spillover step [77] of the Cl• from the Pd site to the Mn site. Somewhat similar mechanism with the heterogeneous recombination of the intermediates on the different kind of sites has been already reported by Furuya and Motoo [84] for the hydrogen evolution reaction on the metal electrodes attaching adatoms.

2. Anodic characteristics of the film-type electrodes of mixed Mn-Pd oxides

Figure 40 shows the anodic polarization curves of the Ti/PdOx(10^{-6}), Ti/MnOx(8×10^{-6})-PdOx(2×10^{-6}) and Ti/MnOx(8×10^{-6})-RuOx(2×10^{-6}) electrodes. The curve for the Ti/MnOx-PdOx electrode is fairly different from that for the Ti/MnOx-RuOx

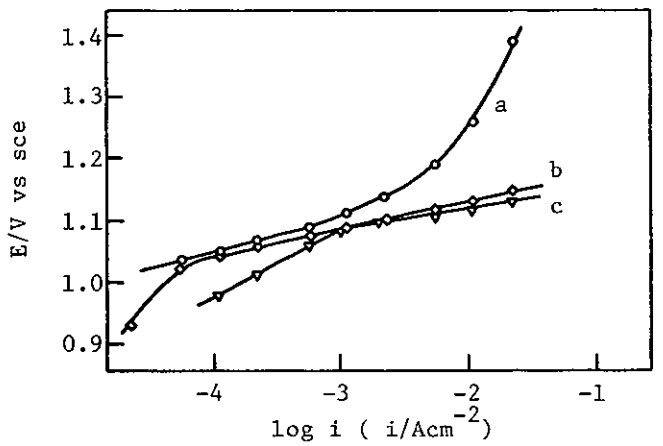

Fig. 40. Current-potential curves of Ti-supported electrodes.
a:Ti/MnOx(8×10^{-6})-PdOx(2×10^{-6})
b:Ti/MnOx(8×10^{-6})-RuOx(2×10^{-6})
c:Ti/PdOx(10^{-6})

electrode and the catalytic activity of the former electrode is much inferior to that of the Ti/PdOx electrode. For these reasons, the followings can be pointed out. In the case of the Ti/PdOx electrode, the active layer consists of PdO and a small amount of metallic Pd [85], which contributes to both the adhesion of the active layer to the Ti substrate and the electric conductivity in the region of the Ti/PdOx interface. On the other hand, in the case of the Ti/MnOx-PdOx electrode, the addition of MnOx in PdOx causes the growth of the insulating TiO_2 on the Ti substrate in the same manner as in the Ti/MnOx electrodes, and the metallic Pd coexisting in the active layer is also oxidized to PdO completely because of the strong oxidizing atmosphere induced by the presence of MnOx. These lead to the decrease in the electric conductivity, and hence the addition of MnOx to PdOx is rather undesirable for the

anodic characteristics of the Ti-supported electrodes. In contrast to the mixed oxides of Mn and Pd, RuOx mainly composed of RuO_2 has a high conductivity [86-88] as well as its high solubility in TiO_2 [3,16,42,44,89] enough to provide the high electric conductivity of the Ti/MnOx-RuOx electrode. Thus, the high catalytic activity of RuOx for the chlorine evolution reaction appears even in the case of the Ti/MnOx-RuOx electrodes. That is to say, the poor electrical property of the Ti/MnOx preferencially appears in that of the Ti/MnOx-PdOx electrodes, while the good electrical and electrochemical properties of the Ti/RuOx are strongly reflected in those of the Ti/MnOx-RuOx electrodes.

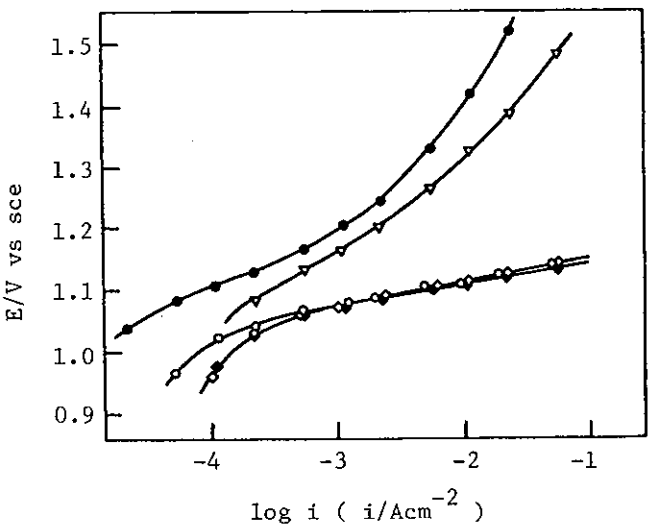

Fig. 41. Current-potential curves of Ti/RuOx-supported electrodes.
- ●:Ti/RuOx(2×10^{-8})
- ▽:Ti/RuOx(2×10^{-8})/MnOx(10^{-5})
- ○:Ti/RuOx(2×10^{-8})/MnOx(10^{-5})-PdOx(10^{-7})
- ◇:Ti/RuOx(2×10^{-8})/MnOx(10^{-8})-PdOx(2×10^{-7})
- ◆:Ti/RuOx(2×10^{-8})/PdOx(2×10^{-7})

In order to minimize the catalytic activity of RuOx in the mixed oxide system, the thermal decomposition was carried out in two stages for the electrode preparation. The Ti substrate was at first coated with thin film of RuOx ($2x10^{-8}$mol/cm^2) and then with layer of MnOx and/or PdOx. The current-potential curves of the resulted electrodes are shown in Fig. 41. The Ti/RuOx($2x10^{-8}$) electrode showed somewhat lower activity owing to the insufficient amount of the catalyst loadings. The Ti/RuOx($2x10^{-8}$)/MnOx(10^{-5}) electrode, whose active layer was predominantly composed of MnOx, was more active than the Ti/RuOx electrodes, but much less active than the PdOx-containing electrode. It is considered that the low chlorine overvoltage of the Ti/RuOx/MnOx-PdOx electrodes is attributable to high electric conductivity of the RuO_2 in the region of the Ti substrate/active layer interface. By comparing the polarization curves of the Ti/RuOx/PdOx and Ti/RuOx/MnOx-PdOx electrodes, however, it became apparent that the existence of MnOx in the catalyst hardly affects the catalytic activity in this system.

The results for the Ti/MnOx-RuOx electrodes shown in Fig. 40 suggest that RuOx coexisting in the Ti/MnOx still keeps high conductivity. Therefore, the improved conductivity could be expected for the Ti/MnOx-PdOx-RuOx electrodes if they were prepared by the simultaneous thermal decomposition of mixed solutions of $Mn(NO_3)_2$, $PdCl_2$ and $RuCl_3$. The polarization curves of the resulted electrode and the relating electrodes are shown in Fig. 42. The amounts of PdOx loadings are 10^{-7} mol/cm^2, while that of MnOx loading is 10^{-5}mol/cm^2. It is evident from this figure that the PdOx existing in the active

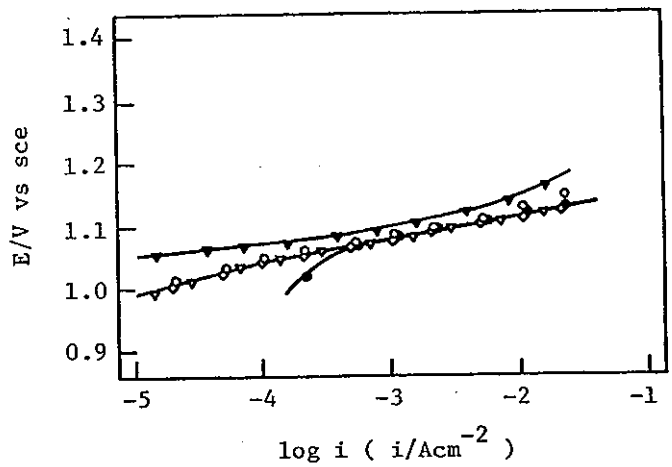

Fig. 42. Current-potential curves of massive and Ti-supported electrodes.
▼:tablet-type PdO
▽:massive MnO_2-Pd(2)
○:Ti/MnOx(10^{-5})-PdOx(10^{-7})-RuOx(10^{-7})
●:Ti/PdOx(10^{-7})
◇:Ti/PdOx(10^{-7})-RuOx(10^{-7})

layer specially serves as an active catalyst for the anodic evolution of chlorine. Though it has already been well-known that RuO_2 is one of the most active catalysts for this reaction [11-22], any decrease in the overvoltage by addition of RuOx in PdOx was not observed on the Ti/PdOx-RuOx electrode. The data on the massive MnO_2 electrodes, included in Fig. 42, showed that the activity of the massive MnO_2 doped with 2atom.% Pd, MnO_2-Pd(2) electrode, was superior to that of the tablet-type pure PdO electrode. However, the expected synergistic effects were not observed in the case of the film-type electrodes. Such different results are probably due to the difference in dispersing conditions of Pd (or PdOx) and specific surface areas of catalysts. It is also possible to consider that the TiO_2

formed in the Ti/PdOx electrode plays the role which the MnO_2 does in the massive MnO_2-Pd electrode. That is, the Pd site might be dispersed in a relatively small amount of the TiO_2 on the substrate, in analogy with the Pd in the massive MnO_2.

Consequently, any unambiguous evidence of synergistic effects was not observed in the film-type Mn-Pd mixed oxide electrodes because of the complexity of the electrode system. However, it was at least suggested from the results obtained with the massive electrodes that more effective configuration of the active sites becomes feasible by introducing the active catalyst into inactive one. Thus, from these viewpoints, the introduction of other components into various kinds of oxides will be investigated with great interest.

4. SUMMARY

The electrocatalytic activities of the mixed Mn-Pd oxides were examined for the chlorine evolution reaction. The results obtained in this chapter are summarized as follows.

1. A second order relation observed on the massive MnO_2-Pd between the rate of the chlorine evolution and the number of the surface Pd sites suggested strongly that the active sites are more effectively dispersed on the MnO_2 surface with microscopic homogeneity.

2. From the data of the activation energies, it was also supported that the reaction mechanism on the lower doped MnO_2-Pd is somewhat different from that on the pure PdO electrode.

3. In the case of the film-type Mn-Pd oxides, however, any distinct evidence of synergistic effects was not observed because of the complexity of the electrode system and of the high activity of the PdOx film itself.

CONCLUSION

The author carried out the studies on the anodic characteristics of manganese oxides in aqueous solutions. The main results and conclusions obtained in this work are summarized as follows.

1. The film-type manganese oxides, MnOx, supported with conductive substrates such as Pt and RuOx-coated Ti exhibit a relatively high activity for the anodic evolution of oxygen. The process of the primary water or hydroxide ion discharge is rate-determining in the oxygen evolution reaction on the MnOx film electrodes.

2. The redox reaction of Mn(III)/Mn(IV) in the massive manganese oxides is characterized by accompanying the diffusion of H^+ ions in the solid phase. The active site for the oxygen and chlorine evolution reaction is regarded as the Mn(III) site at the surface, and the oxidation process of the Mn(III) site is considered to be a common rate-determining step in both reactions on the massive manganese oxides.

3. The doping of small amounts of noble metals, especially Pd, in the massive β-MnO_2 decreases the chlorine overvoltage enomously. The kinetic data suggest that the surface sites of the doped metals serve as an active site for the chlorine evolution reaction.

4. In the case of the massive MnO_2-Pd electrodes, the active Pd sites are effectively dispersed on the MnO_2 surface with microscopic homogeneity, and the kinetics of the chlorine

evolution reaction, especially on the lower Pd-doped MnO_2, is somewhat different from that on the pure PdO electrode. In the case of the film-type Mn-Pd mixed oxides, however, the catalytic activity is not improved by mixing of the oxides.

ACKNOWLEDGMENT

The research based on this thesis was carried out at Department of Applied Chemistry, Faculty of Engineering, Osaka University.

The work was supervised by Professor Dr. Hideo Tamura, to whom I am deeply indebted for his invaluable guidance and continuous encouragement throughout this work.

I am also very much obliged to Assistant Professor Dr. Chiaki Iwakura for his numerous fruitful discussions and helpful suggestions in the course of this thesis and for kindful suggestions to prepare the manuscripts.

I am very grateful to Associate Professor Dr. Hiroshi Yoneyama and Mr. Osamu Ikeda for their encouragement and helpful advices.

Finally, I wish to thank all the members of Tamura Laboratory and all my friends for their friendships.

REFERENCES

1. A.T. Kuhn and P.M. Wright, "Industrial Electrochemical Processes" (ed. by A.T. Kuhn), p. 525, Elsevier Pub. Co., New York (1971).
2. eg. H.B. Beer, Belg. Pat. 710,551 (1968); O.de Nora, South African Pat. 68/7371, 68/7482 (1968).
3. O.de Nora, Chem. Ing. Techn., 42, 222 (1970).
4. G. Bianchi, J. Appl. Electrochem., 1, 231 (1971).
5. I.E. Veselovskaya, L.V. Morochko, L.I. Yurkov and L.M. Yakimenko, Élektrokhimiya, 10, 1017 (1974).
6. G. Faita, P. Longhi and T. Mussini, J. Electrochem. Soc., 114, 340 (1967).
7. G. Faita, G. Fiori and J.W. Augustynski, J. Electrochem. Soc., 116, 928 (1969).
8. G. Faita, G. Fiori and A. Nidora, J. Electrochem. Soc., 117, 1333 (1970).
9. R.T. Atanasoski, B.Ž. Nikolić, M.M. Jakšić and A.R. Despić, J. Appl. Electrochem., 5, 155 (1975).
10. T. Arikado, C. Iwakura and H. Tamura, Electrochim. Acta, 22, 229 (1977).
11. G. Faita and G. Fiori, J. Appl. Electrochem., 2, 31 (1972).
12. E.A. Kalinovskii, R.U. Bondar' and N.N. Meshkova, Élektrokhimiya, 8, 1468 (1972).
13. R.G. Erenburg, L.I. Kristalik and V.I. Bystrov, Élektrokhimiya, 8, 1740 (1972).
14. V.I. Bystrov, Élektrokhimiya, 11, 1902 (1975).

15. N.Ya. Bunĕ, G.A. Shilyaeva and V.V. Losev, Élektrokhimiya, 13, 1540 (1977).

16. F. Hine, M. Yasuda and T. Yoshida, J. Electrochem. Soc., 124, 500 (1977).

17. L.J.J. Janssen, L.M.C. Starmans, J.G. Visser and E. Barendrecht, Electrochim. Acta, 22, 1093 (1977).

18. T. Arikado, C. Iwakura and H. Tamura, Electrochim. Acta, 23, 9 (1978).

19. J. Augustynski, L. Balsenc and J. Hinden, J. Electrochem. Soc., 125, 1093 (1978).

20. I.R. Burrows, D.A. Denton and J.A. Harrison, Electrochim. Acta, 23, 493 (1978).

21. D.A. Denton, J.A. Harrison and R.I. Knowles, Electrochim. Acta, 24, 521 (1979).

22. L.D. Burke and J.F. O'Neill, J. Electroanal. Chem., 101, 341 (1979).

23. M. Takahashi and N. Masuko, "Kogyodenkai no Kagaku", Chap. 9, Agune, Tokyo (1979).

24. W. O'Grady, C. Iwakura, J. Huang and E. Yeager, "Proceedings of the Symposium on Electrocatalysts" (ed. by M.W. Breiter), p. 286, The Electrochemical Society, New Jersey (1974); Technical Report, No. 37, Case Western Reserve University, 1 May (1974).

25. C. Iwakura, K. Hirao and H. Tamura, Electrochim. Acta, 22, 335, (1977).

26. C. Iwakura, H. Tada and H. Tamura, Denki Kagaku, 45, 202 (1977).

27. L.D. Burke, O.J. Murphy, J.F. O'Neill and S. Venkatesan, J. Chem. Soc. Faraday 1, 73, 1659 (1977).

28. G. Lodi, E. Sivieri, A.de Battisti and S. Trasatti, J. Appl. Electrochem., 8, 135 (1978).

29. D.V. Kokoulina, Yu.I. Krasovitskaya and T.V. Ivanova, Élektrokhimiya, 14, 470 (1978).

30. M.A. Malati, Chem. Ind. (London), 17, 446 (1971).

31. W.C. Vosburg, J. Electrochem. Soc., 106, 839 (1959); A. Kozawa and R.A. Powers, J. Electrochem.Soc., 113, 870 (1966); C.C. Liang, "Encyclopedia of Electrochemistry of the Elements" (ed. by A.J. Bard), Vol. I, Chap. 6, p. 349, Marcel Dekker, Inc., New York (1973).

32. G.N. Kokhanov, R.A. Anganova and N.G. Milova, Élektrokhimiya, 8, 862 (1972).

33. E.M. Shembel', E.A. Kalinovskii, V.L. Moskalevich, O.M. Mazur and V.G. Artamonov, Élektrokhimiya, 8, 1351 (1972).

34. E.A. Kalinovskii, V.A. Shustrov, V.M. Chaikovskaya and O.L. Prusskaya, Élektrokhimiya, 12, 1573 (1976).

35. A.K. Gorbachev, É.É. Krench and V.I. Shmorgun, Élektrokhimiya, 13, 1046 (1977).

36. R. Mráz, V. Srb and S. Tichý, Electrochim. Acta, 18, 551 (1973).

37. M.B. Konovalov, E.A.Kalinovskii, A.F. Nikiforov and V.V. Stender, Khim. Teknologiya, 17, 101 (1971).

38. C. Iwakura, K. Fukuda and H. Tamura, Electrochim. Acta, 21, 501 (1976).

39. A.K. Covington, T. Cressey, B.G. Lever and H.R. Thirsk, Trans. Faraday Soc., 58, 1975 (1962).

40. A. Kozawa and W.C. Vosburgh, J. Electrochem. Soc., 105, 59 (1958).

41. C. Butler and H.R. Thirsk, J. Electrochem. Soc., 100, 297, (1953).

42. I.E. Veselovskaya, E.K. Spasskaya, V.A. Sokolov, V.I. Tkachenko and L.M. Yakimenko, Élektrokhimiya, 10, 70, (1974).

43. H. Tamura, H. Yoneyama, C. Iwakura and T. Murai, Bull. Chem. Soc. Jpn., 50, 753 (1977).

44. K. Fukuda, C. Iwakura and H. Tamura, Abstract(1K45) presented at 36th Spring Meeting of the Chemical Society of Japan, April (1977).

45. M. Valigi and A. Cimino, J. Solid State Chem., 12, 135 (1974).

46. "The Oxide Handbook" (ed. by G.V. Samsonov), p. 25,28, Plenum Pub. Co., New York (1973).

47. "Kagaku Binran" (ed. by Chemical Society of Japan), p. 1423, Maruzen, Tokyo (1975).

48. H.Y. Kang and C.C. Liang, J. Electrochem. Soc., 115, 6 (1968).

49. H.S. Harned and M.A. Cook, J. Am. Chem. Soc., 59, 496 (1937).

50. J.O'M. Bockris, J. Chem. Phys., 24, 817 (1956).

51. A. Damjanovic, A. Dey and J.O'M. Bockris, Electrochim. Acta, 11, 791 (1966).

52. Y. Yoneda, J. Electrochem. Soc. Japan, 22, 266 (1949).

53. A. Hickling and S. Hill, Discuss. Faraday Soc., 1, 236 (1947).

54. R. Naumann, Ch. Hirche and G. Wolf, Z. Phys. Chem., 257, 697 (1976).

55. J.S. Wiley and H.T. Knight, J. Electrochem. Soc., 111, 656 (1964).

56. P.H. Klose, J. Electrochem. Soc., 117, 854 (1970).

57. T. Arikado, C. Iwakura and H. Tamura, Electrochim. Acta, 22, 513 (1977).

58. R.S. Nicholson and I. Shain, Analyt. Chem., 36, 706 (1964).

59. H.R. Thirsk and J.A. Harrison, "A Guide to the Study of Electrode Kinetics", Chap. 2, p. 52, Academic Press, London (1972).

60. T. Valand, Electrochim. Acta, 19, 639 (1974).

61. J.J. Larange and J. Brenet, Bull. Soc. Chim. Fr., 7, 2455 (1970).

62. A.B. Scott, J. Electrochem. Soc., 107, 941 (1960).

63. G. Faita, G. Fiori and T. Mussini, Electrochim. Acta, 13, 1765 (1968).

64. T. Yokoyama and M. Enyo, Abstract(A124) presented at the 43rd Annual Meeting of the Electrochemical Society of Japan, April (1976).

65. S.M. Ahmed and D. Maksimov, Can. J. Chem., 46, 3841 (1968).

66. A. Kozawa, Abstract(D116) presented at the 44th Annual Meeting of the Electrochemical Society of Japan, April (1977).

67. S. Gottesfeld and S. Srinivasan, J. Electroanal. Chem., 86, 89 (1978).

68. G. Singh, M.H. Miles and S. Srinivasan, "Electrocatalysis on Non-Metallic Surfaces" (ed. by A.D. Franklin), p. 289, National Bureau of Standards, Maryland (1976).

69. M. Takahashi, Hyomen, 12, 170 (1974).

70. F.A. Cotton and G. Wilkinson, "Advanced Inorganic Chemistry" Chap. 30, Wiley, New York (1966).

71. A. Kozawa, J. Electrochem. Soc., 106, 552 (1959).

72. I.R. Burrows, J.H. Entwisle and J.A. Harrison, J. Electroanal. Chem., 77, 21 (1977).

73. J.H. Sluyters, Rec. Trav. Chim., 79, 1092 (1960).

74. M.R. Andrew, J.S. Drury, B.D. McNicol, C. Pinnington and R.T. Short, J. Appl. Electrochem., 6, 99 (1976).

75. C. Iwakura, M. Inai and H. Tamura, Chem. Lett., 1979, 225 (1979).

76. J.H. Fishman, J.F. Henry and S. Tessor, Electrochim. Acta, 14, 1314 (1969).

77. J.O'M. Bockris and J. McHardy, J. Electrochem. Soc., 120, 61 (1973).

78. T.A. Chertykovtseva, Z.D. Skuridina, D.M. Shub and V.I. Veselovskii, Élektrokhimiya, 14, 1412 (1978).

79. Ya.M. Kolotyrkin, Extended abstract(No. 19) presented at the 3rd Japan-USSR Seminar on Electrochemistry, Kyoto, December, 1978; Denki Kagaku, 47, 390 (1979).

80. D. Cipris and D. Pouli, J. Electroanal. Chem., 73, 125 (1976).

81. L.M. Elina, V.M. Gitneva and V.I. Bystrov, Élektrokhimiya, 11, 1279 (1975).

82. B.E. Conway and D.M. Novak, J. Electroanal. Chem., 99, 133 (1979).

83. T. Arikado, C. Iwakura and H. Tamura, Electrochim. Acta, 23, 799 (1978).

84. N. Furuya and S. Motoo, J. Electroanal. Chem., 88, 151 (1978).

85. K. Ooe, Y. Kawai and S. Saito, Abstract(B311) presented at the 42nd Annual Meeting of the Electrochemical Society of Japan, April (1975).

86. D.B. Rogers, R.D. Shannon, A.W. Sleight and J.L. Gillson, Inorg. Chem., 8, 841 (1969).

87. S. Pizzini, G. Buzzanca, C. Mari, L. Rossi and S. Torchio, Mat. Res. Bull., 7, 449 (1972).

88. D. Galizziori, F. Tantardini and S. Trasatti, J. Appl. Electrochem., 5, 203 (1975).

89. W.A. Gerrard and B.C.H. Steele, J. Appl. Electrochem., 8, 417 (1978).